Me-Talnetant and Osanetant Interact within Overlapping but Not Identical Binding Pockets in the Human Tachykinin Neurokinin 3 Receptor Transmembrane Domains

Pari Malherbe, Caterina Bissantz, Anne Marcuz, Claudia Kratzeisen, Marie-Thérèse Zenner, Joseph G. Wettstein, Hasane Ratni, Claus Riemer, and Will Spooren

Psychiatry Disease Area (P.M., A.M., C.K., M.-T.Z., J.G.W., W.S.) and Chemistry Discovery (C.B., H.R., C.R.), F. Hoffmann-La Roche Ltd., Basel, Switzerland

ABSTRACT

Recent clinical trials have indicated that neurokinin 3 receptor antagonists (S)-(+)-N-{{3-[1-benzoyl-3-(3,4-dichlorophenyl)-piperidin-3-yl]prop-1-yl}-4-phenylpiperidin-4-yl}-N-methylacetamine (SR142801; osanetant) and (S)-(−)-N-(α-ethylbenzyl)-3-hydroxy-2-phenylquinoline-4-carboxamide (SB223412; talnetant) may treat symptoms of schizophrenia. Using site-directed mutagenesis, rhodopsin-based modeling, [^{3}H](S)-(−)-N-(α-ethylbenzyl)-3-methoxy-2-phenylquinoline-4-carboxamide (Me-talnetant) and [^{3}H]osanetant binding, and functional Schild analyses, we have demonstrated the important molecular determinants of neurokinin B (NKB), Me-talnetant, and osanetant binding pockets. The residues Asn138$^{2.57}$, Asn142$^{2.61}$, Leu232$^{45.49}$, Tyr315$^{6.51}$, Phe342$^{7.39}$, and Met346$^{7.43}$ were found to be crucial for the NKB binding site. We observed that the M134$^{2.53}$A, V169$^{3.36}$M, F342$^{7.39}$M, and S341$^{7.38}$I/F342$^{7.39}$M mutations resulted in the complete loss of [^{3}H]Me-talnetant and [^{3}H]osanetant binding affinities and also abolished their functional potencies in an NKB-evoked accumulation of [^{3}H]inositol phosphates assay, whereas the mutations V95$^{1.42}$A, N142$^{2.61}$A, Y315$^{6.51}$F, and M346$^{7.43}$A behaved differently between the interacting modes of two antagonists. V95$^{1.42}$A and M346$^{7.43}$A significantly decreased the affinity and potency of Me-talnetant. Y315$^{6.51}$F, although not affecting Me-talnetant, led to a significant decrease in affinity and potency of osanetant. The mutation N142$^{2.61}$A, which abolished the potency and affinity of osanetant, led to a significant increase in the affinity and potency of Me-talnetant. The proposed docking mode was further validated using (S)-2-(3,5-bis-trifluoromethyl-phenyl)-N-[4-(4-fluoro-2-methyl-phenyl)-6-((S)-4-methanesulfonyl-3-methyl-piperazin-1-yl)-pyridin-3-yl]-N-methyl-isobutyramide (RO49085940), from another chemical class. It is noteworthy that the mutation F342$^{7.39}$A caused an 80-fold gain of RO4908594 binding affinity, but the same mutation resulted in the complete loss of the affinity of Me-talnetant and partial loss of the affinity of osanetant. These observations show that the binding pocket of Me-talnetant and osanetant are overlapping, but not identical. Taken together, our data are consistent with the proposed docking modes where Me-talnetant reaches deeply into the pocket formed by transmembrane (TM)1, -2, and -7, whereas osanetant fills the pocket TM3, -5, and -6 with its phenyl-piperidine moiety.

The tachykinin family comprises the neuropeptides substance P (SP; RPKPQQFFGLM-NH2), neurokinin A (NKA; HKTDSFVGLM-NH2), and neurokinin B (NKB; DMHD-FFVGLM-NH2), which share a common C-terminal sequence, FXGLM-NH2. SP, NKA, and NKB act as neurotransmitters or neuromodulators, and they elicit their effects through three types of neurokinin receptors: NK_1R, NK_2R, and NK_3R, respectively. Neurokinin receptors (NKRs) belong to the superfamily of G protein-coupled receptors (GPCRs) that couple via $G_{q/11}$ to the activation of phospholipase C, leading to elevation of intracellular Ca^{2+} levels (Severini et al., 2002; Almeida et al., 2004; Beaujouan et al., 2004). NKRs

ABBREVIATIONS: SP, substance P; NK, neurokinin; NKR, neurokinin receptor; GPCR, G protein-coupled receptor; 3D, three-dimensional; Me-talnetant, (S)-(−)-N-(α-ethylbenzyl)-3-methoxy-2-phenylquinoline-4-carboxamide); osanetant, SR142801, (S)-(+)-N-{{3-[1-benzoyl-3-(3,4-dichlorophenyl)piperidin-3-yl]prop-1-yl}-4-phenylpiperidin-4-yl}-N-methylacetamine; SB222200, (S)-(−)-N-(α-ethylbenzyl)-3-methyl-2-phenylquinoline-4-carboxamide; talnetant, SB223412, (S)-(−)-N-(α-ethylbenzyl)-3-hydroxy-2-phenylquinoline-4-carboxamide; RO4908594, (S)-2-(3,5-bis-trifluoromethyl-phenyl)-N-[4-(4-fluoro-2-methyl-phenyl)-6-((S)-4-methanesulfonyl-3-methyl-piperazin-1-yl)-pyridin-3-yl]-N-methyl-isobutyramide; IP, inositol phosphates; h, human; TM, transmembrane; EC2, extracellular loop 2; I3, intracellular loop 3; HEK, human embryonic kidney; RT, room temperature; PBS, phosphate-buffered saline; CHO, Chinese hamster ovary; WT, wild type; HBSS, Hanks' balanced salt solution; 7TMD, seven-transmembrane domain; SAR, structure-activity relationship(s); 3D, three-dimensional; AVP, arginine vasopressin; V_1R, vasopressin 1 receptor.

have been implicated in the pathology of psychiatric diseases such as depression, schizophrenia, and anxiety as well as other conditions, including asthma, pain, emesis, and arthritis (Albert, 2004). Among the NKRs, the NK$_3$R is of particular interest because of its brain distribution and its possible role in the pathophysiology of psychiatric disorders, including schizophrenia (Spooren et al., 2005; Meltzer and Prus, 2006). Senktide, which is a synthetic peptide, has been found to be a highly selective and potent agonist at the NK$_3$R. Based on in situ hybridization histochemistry, and NKB/senktide binding, the expression of NK$_3$R was detected in brain regions that include cortex (frontal, parietal, and cingulate cortex), various nuclei of the amygdala, the hippocampus, and midbrain structures (substantia nigra, ventral tegmental area, and raphe nuclei) (Stoessl, 1994; Shughrue et al., 1996; Langlois et al., 2001). Note that at the cellular level, NK$_3$R is found on the cell surface of the A9 and A10 dopamine cell groups in the midbrain (Stoessl, 1994; Langlois et al., 2001).

Various preclinical studies have demonstrated the involvement of NK$_3$R-mediated activation in the release of dopamine, especially in ventral and dorsal striatal regions. Furthermore, recent phase II clinical results with osanetant and talnetant, NK$_3$R antagonists from two distinct chemical classes, have indicated beneficial effect for the treatment of schizophrenia (Meltzer et al., 2004; Spooren et al., 2005; Meltzer and Prus, 2006; Dawson et al., 2007). Osanetant was the first potent nonpeptide antagonist of the NK$_3$R to be reported (Emonds-Alt et al., 1995; Nguyen-Le et al., 1996). Talnetant was subsequently described (Sarau et al., 1997; Giardina et al., 1999). Information about phase II clinical trial of osanetant, the only data that have been published in detail thus far, showed the compound to be active in schizophrenia patients with improved efficacy, side effect profiles, and good tolerability (Meltzer et al., 2004). Therefore, potent and selective NK$_3$R antagonists have recently attracted special attention over the current mainstay treatments with antipsychotic drugs, offering an alternative therapeutic for psychiatric disorders such as schizophrenia and bipolar syndrome.

Although talnetant clearly displayed a reversible and competitive mode of antagonism in the NKB-induced Ca^{2+} mobilization at cloned hNK$_3$R and in the senktide-induced contractions in rabbit isolated iris sphincter muscles (Sarau et al., 1997; Giardina et al., 1999), there have been conflicting reports regarding the inhibition mode of osanetant. Investigations using [MePhe^7]NKB- and senktide-stimulated inositol phosphates (IP) formation at the cloned hNK$_3$R (Oury-Donat et al., 1995) or [MePhe^7]NKB-mediated contractions of guinea pig ileum (Emonds-Alt et al., 1995) have shown a competitive mode of antagonism by osanetant. However, other studies that used senktide- and [MePhe^7]NKB-mediated contractions of the guinea pig ileum (Patacchini et al., 1995; Nguyen-Le et al., 1996) or senktide-induced formation of [^{3}H]IP in slices from the guinea pig ileum (Beaujouan et al., 1997) pointed to a noncompetitive and long-lasting irreversible antagonism by osanetant. A recent study, which compared antagonism modes of talnetant and osanetant in cellular Ca^{2+} mobilization and binding kinetics, has demonstrated that both antagonists displayed similar binding kinetics notwithstanding the abnormal Schild plot of osanetant in the functional Ca^{2+} mobilization assay (Tian et al., 2007).

Although the residues in the orthosteric binding site of NK$_1$R and NK$_2$R involved in the interaction with endogenous agonist peptides or nonpeptide antagonists have been extensively characterized (Almeida et al., 2004), little is known about NK$_3$R ligand binding pocket, except for one report (Wu et al., 1994) showing the involvement of TM2 residues Met134 and Ala146 in the species-selectivity of SR48968 (a close derivative of osanetant) for hNK$_3$R. The current research used a combination of three-dimensional (3D)-modeling, site-directed mutagenesis, [^{3}H]Me-talnetant and [^{3}H]osanetant bindings, [MePhe^7]NKB-stimulated IP formation, and Schild and kinetic analyses to identify the important molecular determinants of NKB, Me-talnetant, and osanetant binding pockets and to elucidate the antagonism mode of both antagonists on wild-type and mutated hNK$_3$Rs. Furthermore, these experimental findings allow the construction of a homology model based on the X-ray crystal of bovine rhodopsin (Palczewski et al., 2000), and they suggest possible binding modes for Me-talnetant and osanetant.

Materials and Methods

Materials. Me-talnetant, osanetant (SR142801), SB222200, talnetant (SB223412), and RO4908594 were synthesized within the Chemistry Department of F. Hoffmann-La Roche (Basel, Switzerland). [^{3}H]Me-talnetant (specific activity, 84.6 Ci/mmol) was synthesized at the Roche Chemical and Isotope Laboratories. [^{3}H]Osanetant ([^{3}H]SR142801; specific activity, 74.0 Ci/mmol) was purchased from GE Healthcare (Chalfont St. Giles, UK). [MePhe^7]Neurokinin B (Asp-Met-His-Asp-Phe-Phe-NMe-Phe-Gly-Leu-Met-NH$_2$) was purchased from NeoMPS SA (Strasbourg, France).

Construction of Point-Mutated hNK$_3$Rs. cDNA encoding the human NK$_3$R (accession no. P29371) was subcloned into pCI-Neo expression vectors (Promega, Madison, WI). All point-mutants were constructed using the QuikChange site-directed mutagenesis kit (Stratagene, La Jolla, CA) according to the manufacturer's instructions and using pCI-Neo-hNK$_3$R as a DNA template. Complementary oligonucleotide primers (sense and antisense) containing the single site or double sites of mutations were synthesized by Microsynth AG (Balgach, Switzerland). The following polymerase chain reaction conditions were used for repeated extensions of the plasmid template: 95°C for 1 min and 20 cycles of 95°C for 30 s, 55°C for 1 min, and 68°C for 8 min using 50 ng of plasmid DNA, 100 ng of each primer, and 2.5 units of *Pfu* Turbo DNA polymerase (Stratagene). The entire coding regions of all positive point-mutants were sequenced from both strands using an automated cycle sequencer (Applied Biosystems, Foster City, CA).

Cell Culture, Large-Scale Transient Transfection, and Membrane Preparation. Human embryonic kidney (HEK) 293-EBNA cells (Invitrogen, Carlsbad, CA) were adapted to grow in suspension in spinner flasks at 95 to 105 rpm. For transfection experiments, we used a modified medium (DHI special; Invitrogen) and for the gene delivery, we used transfection reagent X-tremeGENEQ$_2$ (Roche Applied Science, Rotkreuz, Switzerland), which consists of substances A and B. Cells were cultured to a density of 6 to 10 × 10^5 cells/ml, centrifuged for 3 min at 600 rpm, and resuspended in DHI media. The cell density was adjusted to 5 × 10^5 cells/ml, and the culture was incubated for at least 3 h before transfection. The transfection complexes were generated in 1/10 of the culture volume in DHI media at room temperature (RT). For 1 ml of culture, first 0.4 μg of DNA was added to 0.1 ml of medium, mixed, after 2 min followed by 0.15 μg of X-tremeGENEQ A, mixed, and followed after a further 2 min by 0.5 μg of X-tremeGENEQ B. The mixture was incubated for 15 min at room temperature to allow DNA complex formation before it was added to the cells. Forty-eight hours after transfection, the cells were harvested and washed three times

with ice-cold PBS, and then they were frozen at $-80°C$. The pellet was suspended in ice-cold 50 mM Tris, pH 7.4, buffer containing 10 mM EDTA ($10\times$ volume) and homogenized with a Polytron homogenizer (Kinematica AG, Basel, Switzerland) for 30 s at 16,000 rpm. After centrifugation at $48,000g$ for 30 min at 4°C, the pellet was suspended again in ice-cold 10 mM Tris, pH 7.4, buffer containing 0.1 mM EDTA ($10\times$ volume), homogenized, and spun again as described above. The pellet was resuspended in ice-cold 10 mM Tris, pH 7.4, buffer containing 0.1 mM EDTA and 10% sucrose ($5\times$ volume). After homogenization for 15 s at 16,000 rpm, the protein content was measured using the bicinchoninic acid method (Pierce, Socochim, Lausanne, Switzerland), with bovine serum albumin as the standard. The membrane homogenate was frozen at $-80°C$ before use.

[³H]Me-talnetant and [³H]Osanetant Bindings. After thawing, the membrane homogenates were centrifuged at $48,000g$ for 10 min at 4°C, the pellets were resuspended in the binding buffer (50 mM Tris-HCl, 4 mM $MnCl_2$, 1 μM phosphoramidon, and 0.1% bovine serum albumin at pH 7.4) to a final assay concentration of 5 μg of protein/well. Saturation isotherms were determined by addition of various concentrations of [³H]Me-talnetant (0.005–10 nM) or [³H]-osanetant (0.009–3 nM) to these membranes (in a total reaction volume of 500 μl) for 75 min at RT. At the end of the incubation, membranes were filtered onto unitfilter (96-well white microplate with bonded GF/C filter preincubated 1 h in 0.3% polyethylenimine + 0.3% bovine serum albumin; PerkinElmer Life and Analytical Sciences, Waltham, MA) with a FilterMate-96 harvester (PerkinElmer Life and Analytical Sciences) and washed four times with ice-cold 50 mM Tris-HCl, pH 7.4, buffer. Nonspecific binding was measured in the presence of 10 μM SB222200 for both radioligands. The radioactivity on the filter was counted (5 min) on a TopCount microplate scintillation counter (PerkinElmer Life and Analytical Sciences) with quenching correction after addition of 45 μl of MicroScint 40 (PerkinElmer Life and Analytical Sciences) and shaking for 1 h. Saturation experiments were analyzed by Prism 4.0 (GraphPad Software Inc., San Diego, CA) using the rectangular hyperbolic equation derived from the equation of a bimolecular reaction and the law of mass action, $B = (B_{max} \times [F])/(K_d + [F])$, where B is the amount of ligand bound at equilibrium, B_{max} is the maximum number of binding sites, $[F]$ is the concentration of free ligand, and K_d is the ligand dissociation constant. For inhibition experiments, membranes were incubated with [³H]Me-talnetant or [³H]osanetant at a concentration equal to K_d value of radioligand and 10 concentrations of the inhibitory compound (0.0003–10 μM). IC_{50} values were derived from the inhibition curve, and the affinity constant (K_i) values were calculated using the Cheng-Prusoff equation $K_i = IC_{50}/(1 + [L]/K_d)$, where $[L]$ is the concentration of radioligand, and K_d is its dissociation constant at the receptor, derived from the saturation isotherm (Cheng and Prusoff, 1973). To measure association kinetics, membranes were incubated at RT (22°C) in the presence of radioligand ($\sim$1 nM [³H]Me-talnetant or $\sim$0.25 nM [³H]osanetant) for 0, 1, 3, 5, 7, 10, 15, 20, 30, 60, 90, or 120 min, and then the reaction was terminated by rapid filtration. Dissociation kinetics was measured by adding 10 μM SB222200 at different times before filtration to membranes preincubated at RT for 30 min in the presence of $\sim$1 nM [³H]Me-talnetant or for 60 min in the presence of $\sim$0.25 nM [³H]osanetant. Binding kinetics parameters, K_{ob} and K_{off} values (observed on and off rates, respectively), were derived from association-dissociation curves using the one-phase exponential association and decay equations (Prism 4.0), respectively. K_{on}, half-life and K_d were calculated using the $K_{on} = (K_{ob} - K_{off})/[ligand]$, $t_{1/2} = \ln2/K$, and $K_d = K_{off}/K_{on}$ equations, respectively. Statistical significance was determined using a two-tailed t test (Prism 4.0).

[³H]Inositol Phosphates Accumulation Assay. [³H]Inositol phosphates (IP) accumulation was measured as described previously (Malherbe et al., 2006), with the following adaptations. The Chinese hamster ovary (CHO) cells were maintained in Dulbecco's modified Eagle's medium:F-12/Iscove supplemented with 5% dialyzed fetal calf serum and 100 μg/ml penicillin/streptomycin. The CHO cells

were transfected with the wild-type (WT) or mutant hNK₃R cDNAs in pCl-Neo using Lipofectamine Plus reagent (Invitrogen) according to the manufacturer's instructions. Twenty-four hours after transfection, cells were washed twice in labeling medium: Dulbecco's modified Eagle's medium without inositol (MP Biomedicals, Irvine, CA), 10% fetal calf serum, 1% penicillin/streptomycin, and 2 mM glutamate. Cells were seeded at 8×10^4 cells/well in poly-D-lysine–treated 96-well plates in the labeling medium supplemented with 5 μCi/ml [myo-1,2-³H]inositol (specific activity, 16.0 Ci/mmol; GE Healthcare). On the day of assay (48 h after transfection), cells were washed three times with the buffer ($1\times$ HBSS and 20 mM HEPES, pH 7.4) before the addition of agonists or antagonists in assay buffer ($1\times$ HBSS and 20 mM HEPES, pH 7.4, containing 8 mM LiCl, final concentration, to prevent phosphatidyl inositide breakdown). When present, antagonists were incubated for 5 min at RT before stimulation with agonist [MePhe⁷]NKB, at concentrations ranging from 10 μM to 0.1 nM. After 45-min incubation at 37°C with [MePhe⁷]NKB, the assay was terminated by aspiration of the assay buffer and the addition of 100 μl of 20 mM formic acid to the cells. After shaking for 30 min at RT, a 20-μl aliquot was mixed with 80 μl of yttrium silicate beads (12.5 mg/ml; GE Healthcare) that bind to the inositol phosphates (but not inositol) and shaken for 30 min at RT. Assay plates were centrifuged for 2 min at 2500 rpm before counting on a Top-Count microplate scintillation counter with quenching correction (PerkinElmer Life and Analytical Sciences). The relative efficacy (E_{max}) values of [MePhe⁷]NKB was calculated as fitted maximum of the concentration-response curve of each mutated receptors expressed as a percentage of fitted maximum of the WT concentration-response curve from cells transfected and assayed on the same day.

Residue Numbering Scheme. The position of each amino acid residue in the seven transmembrane domain (7TMD) was identified both by its sequence number and by its generic numbering system proposed by Ballesteros and Weinstein (1995), which is shown as superscript. In this numbering system, amino acid residues in the 7TMD are given two numbers; the first number refers to the transmembrane (TM) number, and the second number indicates its position relative to a highly conserved residue of class A GPCRs in that TM, which is arbitrarily assigned 50. The amino acids in extracellular loop 2 (EC2) are labeled 45 to indicate their location between the helices 4 and 5. The highly conserved cysteine thought to be disulfide bonded, was given the index number 45.50, and the residues within the EC2 loop are then indexed relative to the "50" position.

Alignment and Model Building. The amino acid sequences of the human NK₃R (accession no. P29371), rat NK₃R (accession no. P16177), mouse NK₃R (accession no. P47937), gerbil NK₃R (accession no. AM157740), human NK₁R (accession no. P25103), and human NK₂R (accession no. P21452) were retrieved form the Swiss-Prot database. These amino acid sequences were aligned to the sequence of bovine rhodopsin (accession no. P02699) using the ClustalW multiple alignment program (http://www.ebi.ac.uk/clustalw/). A slow pairwise alignment using the BLOSUM matrix series (Henikoff and Henikoff, 1992) and a gap opening penalty of 15.0 were chosen for aligning the amino acid sequences. Other parameters were those given as default. The sequences were aligned in two steps: 1) from the N terminus to the first five residues of the third intracellular loop I3 and 2) from the last five residues of the I3 loop to the C terminus. The I3 loop was excluded from the alignment because it shows too high variability in amino acid composition and length. The alignments were then verified to ensure that conserved residues of the transmembrane regions were aligned and manually adjusted in EC2 to align the conserved cysteine, which takes part in the disulfide bridges occurring between the TM3 segment and EC2.

Using this alignment and the X-ray structure of bovine rhodopsin (Palczewski et al., 2000) as template, the software package MOE (MOE version 2005.05; Chemical Computing Group, Montreal, Quebec, QC, Canada) was used to generate a 3D model of the human NK₃R. Ten intermediate models were generated, and the best model was selected as final MOE model. No minimization was used to keep

the backbone coordinates as in the X-ray structure. After the heavy atoms were modeled, all hydrogen atoms were added in appropriate locations with the preparatory program PROTONATE of AMBER6 (AMBER 6.0; University of California, San Francisco, CA). Osanetant was then manually docked into the transmembrane cavity of the human NK$_3$R model. The docking mode was based on the following hypotheses: 1) the ligand should make a direct interaction with Met134 (2.53) because this residue has been shown to be responsible for species selectivity of SR48968 (Wu et al., 1994); and 2) phenyl-piperidine substructures are privileged fragments for the subpocket formed by the transmembrane domains 3, 5, and 6. The resulting protein-ligand complex was then minimized using AMBER6. The minimization was carried out by 5000 steps of steepest descent followed by conjugate gradient minimization until the root mean square gradient of the potential energy was less than 0.05 kcal/mol Å. A twin cut-off (10.0, 15.0 Å) was used to calculate nonbonded electrostatic interactions at every minimization step, and the nonbonded pair-list was update every 25 steps. A distance-dependent ($\varepsilon = 4r$) dielectric function was used. Removing the ligand from the complex yielded the final coordinates of the human NK$_3$R model. Me-talnetant was then manually docked into the receptor. The proposed docking mode is based on the structure-activity relationships (SAR) of talnetant according to which at position 3 similar side chains as used in the osanetant series can be added. The 3-methoxy group of Me-talnetant has thus to point into the direction of the subpocket TM3, -5, and -6. We additionally docked RO4908594. This compound was previously aligned onto osanetant by comparison of the observed SAR of the osanetant series (Harrison et al., 1998) and the RO4908594 chemical series (Hoffmann et al., 2005). Thus, its docking mode was guided by the docking pose of osanetant and this ligand alignment. Fourteen single point-mutations and three double-mutations of residues surrounding Me-talnetant and osanetant were then chosen for binding and displacement studies to get information about the different residues involved in Me-talnetant and osanetant binding and their selectivity toward hNK$_1$R and hNK$_2$R.

Results

[³H]Me-Talnetant and [³H]Osanetant Binding and Displacement Studies. Talnetant and osanetant have been extensively characterized by in vitro pharmacology; both antagonists potently inhibited [^{125}I]iodohistidyl-[MePhe^7]NKB binding at hNK$_3$R expressed in CHO cells, with K_i values of 1.0 and 0.2 nM, respectively (Emonds-Alt et al., 1995; Sarau et al., 1997; Giardina et al., 1999; Langlois et al., 2001). The structures of talnetant and its central nervous system penetrant analog SB222200 (Sarau et al., 2000) belong to a chemical class different from osanetant (Fig. 1). In the current study, we were interested in the comparison of the binding pockets of these chemically unrelated antagonists of the hNK$_3$R. Although the radioligand [³H]SB222200 is available from GE Healthcare, our in-house binding studies showed that [³H]SB222200 is not a suitable radioligand for in vitro binding because of low specific binding (<20%) in hNK$_3$R-transfected cell membranes, in comparison with [³H]SR142801 ([³H]osanetant), which gave an excellent signal-to-noise ratio of almost 97.5% specific binding in hNK$_3$R cell membranes. Therefore, we have tritiated a close analog of SB222200, termed [³H]Me-talnetant (Fig. 1). To characterize the in vitro binding of [³H]Me-talnetant and [³H]osanetant, saturation binding analyses were performed at binding equilibrium (75-min incubation at RT), as outlined under *Materials and Methods* on membranes isolated from the HEK293-EBNA cells transiently transfected with the hNK$_3$R. The saturation isotherm was monophasic ([³H]Me-

talnetant concentrations of 0.005–10 nM and [³H]osanetant concentrations of 0.009–3 nM) and best fitted to a one-site model for both radioligands (Fig. 2). As seen in Fig. 2, both [³H]Me-talnetant and [³H]osanetant bind to a single saturable site on recombinantly expressed human NK$_3$R (B_{max} of 34.3 and 26.0 pmol/mg protein, respectively), with high affinity (K_d of 0.8 nM and 0.2 nM, respectively). At the K_d values, the nonspecific binding for [³H]Me-talnetant and [³H]osanetant was approximately 6.9 and 2.5% of total bound radioactivity for both radioligands, respectively. Osanetant and SB222200 were able to displace the [³H]Me-talnetant binding from hNK$_3$R membrane, with K_i values of 1.0 ± 0.3 and 5.4 ± 0.5 nM and Hill values of 1.1 ± 0.2 and 0.9 ± 0.0, respectively; and vice versa, Me-talnetant and SB222200 fully displace [³H]osanetant from hNK$_3$R membranes, with K_i values of 5.7 ± 0.3 and 8.7 ± 0.6 nM and Hill values 1.2 ± 0.1 and 1.1 ± 0.1, respectively. Therefore, Me-talnetant shares a common binding pocket in the transmembrane region of the receptor, at least overlapping with that of osanetant.

Of note is the use of two cell systems for binding (HEK293-EBNA cells) and IP accumulation assay (CHO cells) in the current study. Because HEK293-EBNA cells were adapted to grow and be transiently transfected in suspension in spinner flasks, it was possible to produce and prepare the large quantities of transfected cells and membranes required for binding studies. Preliminary experiments with the membranes prepared from both cell systems showed similar K_d values for [³H]Me-talnetant and [³H]osanetant bindings on these membranes, the only difference between these two cell systems being B_{max} values that indicated higher level of expression in HEK293-EBNA cells than that of CHO cells, reflecting the transient transfections. However, because both [³H]Me-talnetant and [³H]osanetant bind to a single site in a saturable manner, the expression level of the receptor does not influence the determination of K_d. The determination of the K_d and the ratio of K_d (mutant)/K_d (WT) is independent of expression levels in the two cell systems. Hence, HEK293-EBNA cells were used for the binding studies.

Alignment of 7TM Domains of the NKRs toward Rhodopsin and Selection of hNK$_3$R Mutations. To elucidate
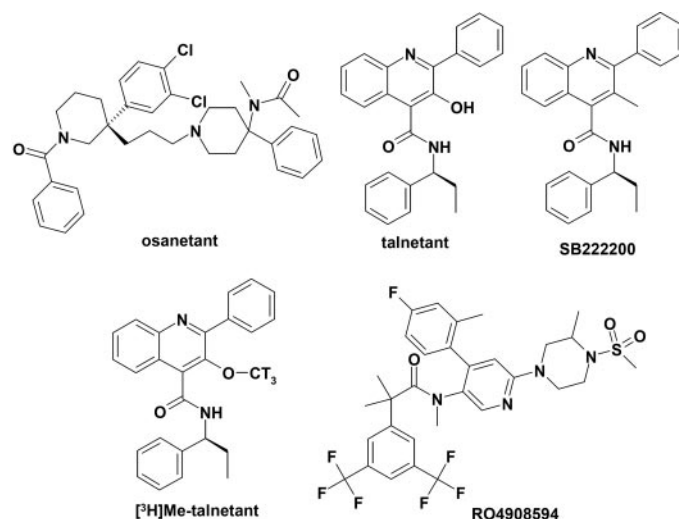
Fig. 1. Chemical structures of NK$_3$R antagonists osanetant (SR142801), talnetant (SB223412), SB222200, and [³H]Me-talnetant and dual NK$_1$R/NK$_3$R antagonist RO4908594. T, tritium.
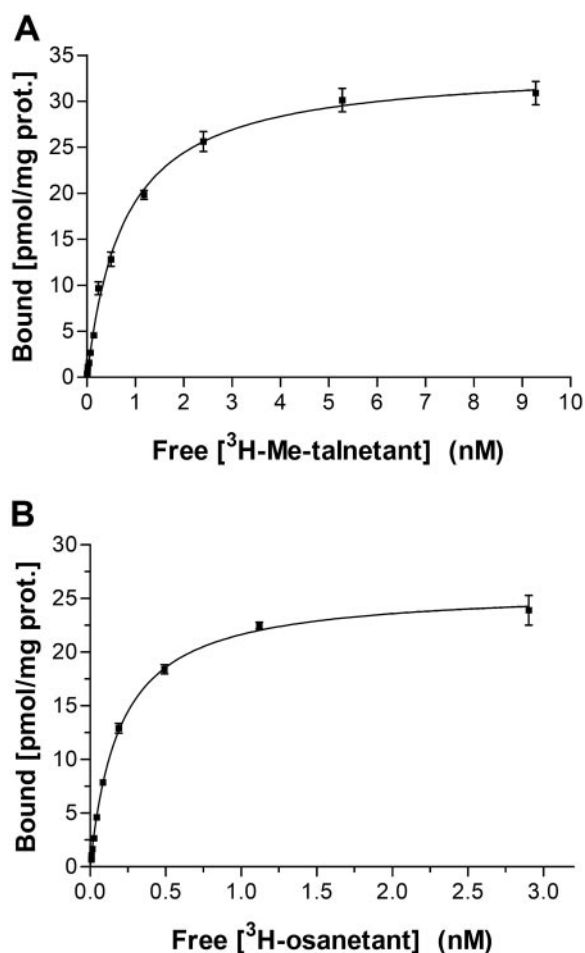
the binding modes of Me-talnetant and osanetant, an alignment of the seven transmembrane helices of the whole NK family toward the transmembrane helices of bovine rhodopsin (Protein Data Bank reference code 1f88) was made. The inverse agonist of rhodopsin, 11-*cis*-retinal, was used as a template for the locations of Me-talnetant and osanetant. Amino acids, which were found 6.0 Å away from retinal in the X-ray crystal structure of rhodopsin (Palczewski et al., 2000), were generally considered as possible candidates to affect bindings of Me-talnetant and osanetant. Because it was reported previously that the residue Met134$^{2.53}$ of hNK$_3$R is responsible for species selectivity of SR48968 (Wu et al., 1994), this information also guided us initially in docking of osanetant. The alignment of these amino acids of the NK family toward rhodopsin is shown in Fig. 3. Comparison of the ligand binding pockets of hNKRs indicated a similarity between the hNK$_3$R and the hNK$_2$R binding pocket (five amino acids different in TM region and EC2 loop, two of them being nonconservative residues), higher than that of hNK$_1$R (eight amino acids different in TM region and EC2 loop, four of them being nonconservative) (Fig. 3). Furthermore, it has been shown that osanetant, talnetant, NKB, and [MePhe^7]-NKB have binding affinities of 744, >100,000, 554, and

Fig. 2. Saturation bindings of [^{3}H]Me-talnetant (A) and [^{3}H]osanetant (B) to membrane preparations from HEK293-EBNA cells transfected transiently with hNK$_3$R. Each data point is mean ± S.E. (bars) of three individual experiments performed in triplicate. The data were analyzed by nonlinear regression analysis using GraphPad Prism 4.0 software and a single-site binding model.

>10,000 nM at hNK$_1$R (in [^{3}H]SP competition binding); 40, 144, 16.5, and 1597 nM at hNK$_2$R (in ^{125}I-NKA binding); and 1.2, 1.0, 0.8, and 0.3 nM at hNK$_3$R (in ^{125}I-[MePhe^7]NKB binding), respectively (Sarau et al., 1997).

For mutational studies, 14 point-mutations and three double mutations located in the TM1, -2, -3, -6, and -7 and EC2 regions (Fig. 3) were selected based on rational outlined below. According to the proposed docking mode, Me-talnetant and osanetant make significant interactions with residues conserved among the three hNKRs. To correctly validate the proposed docking poses, five conserved residues—Met134, Asn138, Asn142, Met346, and Ser348—were mutated to alanine. As Met134 had been shown in the literature to be important for binding of osanetant to hNK$_3$R (Wu et al., 1994), its influence on Me-talnetant was also investigated. Asn138 is close to Met134, forming a pocket that accommodates the ethyl group of Me-talnetant or the benzoyl moiety of osanetant, and it is thus predicted to be a main anchor point for both ligands. Asn142 seems to form a hydrogen bond with Asn138, and it could indirectly influence Me-talnetant and osanetant binding. Met346, according to the docking hypothesis, is important for Me-talnetant but not osanetant; the M346A mutation could therefore be useful for the validation of the hypothesis. Finally, Ser348 could make a hydrogen bond with both ligands.

Subsequently, one of our aims was to address the selectivity of Me-talnetant and osanetant for NK$_3$R over NK$_1$R and NK$_2$R. Although it was not possible to generate all possible mutations of interest, we have chosen a subset of 12 mutants to obtain the information to learn which residues influence selectivity. According to the predicted docking poses, the residues at position 3.36, 6.51, and 7.39 that seem to be important factors for the selectivity of Me-talnetant and osanetant were mutated to the respective residues in hNK$_1$R or hNK$_2$R (V169M, Y315F, and F342M). Phe342 was additionally mutated to alanine, a decision based on the observation that the 4-phenyl substituent of RO4908594 seems to clash into Phe342. Hence, F342A could result in an affinity increase for this compound, an essential test in the validation of the docking poses. NK$_1$R is not only characterized by having a methionine in position 7.39 but also the neighboring residue 7.38 differs from NK$_3$R (serine in NK$_3$R, isoleucine in NK$_1$R). Therefore, the double-mutant S342I/F342M was also generated to correctly introduce the NK$_1$R region in NK$_3$R. The residue at position 7.38 is too far away from the ligands to make a direct interaction with Me-talnetant or osanetant. Nevertheless, although Ser341 is not predicted to be in direct contact with the docked ligands, it could cause a kink of the helix TM7 as a result of its hydrogen-bonding capabilities. Thus, an additional mutant, S341A, was generated. For the case where this mutation would influence Me-talnetant or osanetant binding or the above-mentioned double-mutant would point to an influence of position 7.38 onto binding, single point-mutations S341I (NK$_1$R) and S342L(NK$_2$R) would have to be tested because they could indirectly influence binding by a change of TM7 helix conformation. But these mutations will be no longer be needed in case that S341A does not change the binding affinities.

Comparison of Binding Properties of [^{3}H]Me-Talnetant and [^{3}H]Osanetant to WT and Mutated hNK$_3$Rs. Saturation binding analyses of [^{3}H]Me-talnetant and [^{3}H]-osanetant were performed on membranes isolated from the HEK293-EBNA cells transfected with the WT and mutated

hNK$_3$Rs. The dissociation constants (K_d) and the maximum binding sites (B_{max}) derived from the saturation isotherms are given in Table 1. The mutations V95L, T139A, V95L/T139A, L232A, S341A, and S348A did not significantly affect the binding affinity of both [^{3}H]Me-talnetant and [^{3}H]osanetant compared with the WT hNK$_3$R (Table 1). Four mutations, M134A, V169M, F342M, and S341I/F342M, abolished both [^{3}H]Me-talnetant and [^{3}H]osanetant bindings to undetectable levels (Table 1). Although the mutation N142A abolished [^{3}H]osanetant binding, the same mutation led to an increase in binding affinity of [^{3}H]Me-talnetant by 8-fold that was statistically significant ($P = 0.0047$). The mutation F342A that abolished [^{3}H]Me-talnetant binding affinity led to statistically significant 17-fold decrease in binding affinity of [^{3}H]osanetant ($P = 0.009$). The mutation Y315F, which had no effect on [^{3}H]Me-talnetant binding affinity, led to 9-fold decrease in binding affinity of [^{3}H]osanetant, with high statistical significance ($P = 0.0007$). The binding affinities of [^{3}H]Me-talnetant and [^{3}H]osanetant were decreased by 4.0- and 2.3-fold by mutation V95A, respectively, and they were statistically significant ($P = 0.0002$ and $P = 0.02$). The double-mutation V95I/A99S resulted in decrease in binding affinities of [^{3}H]Me-talnetant and [^{3}H]osanetant by 3.0- and 3.5-fold, which were statistically significant ($P = 0.003$ and $P = 0.009$), respectively. The mutation N138A led to decreases in binding affinities of [^{3}H]Me-talnetant and [^{3}H]-osanetant by 3.5- and 3.8-fold that were statistically significant ($P = 0.004$ and $P = 0.01$). The mutation M346A, which had no effect on [^{3}H]osanetant binding affinity, led to statistically significant 2.5-fold decrease in binding affinity of [^{3}H]Me-talnetant ($P = 0.004$).

Effect of Mutations on the Displacement of [^{3}H]Me-Talnetant by [MePhe^7]NKB, Osanetant, or SB222200. The mutations, which had no effect on or partially affected the [^{3}H]Me-talnetant binding affinity, were chosen further for the competition binding studies with [MePhe^7]NKB, osanetant, and SB222200. Table 2 summarizes the affinity constant (K_i) and Hill slope (n_H) values for the [^{3}H]Me-talnetant displacement by [MePhe^7]NKB, osanetant, or

SB222200 on HEK293-EBNA cell membranes expressing 10 point-mutated and two double-mutated hNK$_3$Rs. In the competitive inhibition of [^{3}H]Me-talnetant binding by [MePhe^7]-NKB, the mutants N138A, L232A, Y315A, and M346A showed 59.4-, 10.0-, 6.2-, and 14.1-fold (statistical significance of $P = 0.0009$, $P = 0.0002$, $P = 0.02$, and $P = 0.006$), respectively, lower affinity for [MePhe^7]NKB than the WT (Fig. 4, A, C, and E; Table 2). The mutation N142A resulted in complete loss of [MePhe^7]NKB binding affinity (Fig. 4C; Table 2). The mutations V95A, V95L, V95I/A99S, T139A, V95L/T139A, S341A, and S348A had no effect on the competition binding by [MePhe^7]NKB (Fig. 4, A, C, and E; Table 2).

As seen in Fig. 4, B, D, and F, and Table 2, the mutations V95A, N138A, N142A, and Y315F that caused decreases in binding affinity of [^{3}H]osanetant (Table 1) resulted similarly to increased affinity constant of osanetant for displacing of [^{3}H]Me-talnetant by 13.6-, 11.2-, 124.3-, and 12.2-fold (statistical significance of $P = 0.04$, $P = 0.0009$, $P = <0.0001$, and $P = 0.005$), respectively. The double-mutant V95I/A99S, which decreased the [^{3}H]osanetant binding affinity by 3.5-fold (Table 1), led to small increase in K_i value of osanetant for displacing of [^{3}H]Me-talnetant (Table 2). SB222200 (a close analog of Me-talnetant) in competition binding assay behaved similarly to Me-talnetant (Table 2). The mutations V95A and N138A caused increases in the K_i values of SB222200 for displacing of [^{3}H]Me-talnetant by 5.0- and 3.9-fold (statistical significance of $P = 0.02$ and $P = 0.04$), respectively. Note that the N142A mutant, which had led to increased binding affinity of [^{3}H]Me-talnetant (Table 1), displayed similarly a 500-fold ($P = 0.0002$) higher affinity for SB222200 in displacing of [^{3}H]Me-talnetant than the WT (Table 2).

Effect of Mutations on the Displacement of [^{3}H]-Osanetant by RO4908594. To further validate the NK$_3$R binding pocket model, another distinct chemical structure, RO4908594 (Fig. 1) was used in a [^{3}H]osanetant competition binding assay. RO4908594 is a potent dual NK$_1$R/NK$_3$R antagonist that binds to hNK$_1$R, hNK$_2$R, and hNK$_3$R, with K_i values of 0.8 ± 0.1, >10,000, and 1.6 ± 0.1 nM, respectively

GPCR	TM1				TM2					TM3								TM4	EC2	TM5						TM6					TM7						
	1.35	1.39	1.42	1.46	2.53	2.57	2.58	2.61	2.65	3.28	3.29	3.32	3.33	3.35	3.36	3.37	3.40	4.60	45.49	5.38	5.39	5.42	5.43	5.46	5.47	6.44	6.48	6.51	6.52	6.55	7.35	7.38	7.39	7.40	7.42	7.43	7.45
NK3R_RAT	W	Y	V	A	V	N	T	N	G	Q	N	P	I	A	V	F	I	Q	L	Y	H	V	I	V	Y	F	W	Y	H	F	Y	S	F	W	A	M	S
NK3R_MOUSE	W	Y	V	A	V	N	T	N	G	Q	N	P	I	A	V	F	I	Q	L	Y	H	V	I	V	Y	F	W	Y	H	F	Y	S	F	W	A	M	S
NK3R_GERBIL	W	Y	V	A	M	N	T	N	A	Q	N	P	I	A	V	F	I	Q	L	Y	H	V	I	V	Y	F	W	Y	H	F	Y	S	F	W	A	M	S
	95	99			134	138	139	142										169		232							315					341	342			346	348	
NK3R_HUMAN	**W**	**Y**	**V**	**A**	**M**	**N**	**T**	**N**	**A**	**Q**	**N**	**P**	**I**	**A**	**V**	**F**	**I**	**Q**	**L**	**Y**	**H**	**V**	**I**	**V**	**Y**	**F**	**W**	**Y**	**H**	**F**	**Y**	**S**	**F**	**W**	**A**	**M**	**S**
NK1R_HUMAN	W	Y	I	S	M	N	T	N	A	H	N	P	I	A	V	F	I	Q	V	Y	H	V	T	I	Y	F	W	F	H	F	Y	I	M	W	A	M	S
NK2R_HUMAN	W	Y	L	A	M	N	A	N	A	Q	N	P	I	A	M	F	I	Q	K	Y	H	V	I	I	Y	F	W	Y	H	F	Y	L	F	W	A	M	S
OPSD_BOVIN	L	M	L	G	M	G	F	T	S	E	G	A	T	G	G	E	L	P	S	F	V	M	F	H	F	F	W	Y	A	A	M	P	A	F	A	K	S

Fig. 3. Alignment of the amino acids forming the binding site. The first row gives the Ballesteros-Weinstein numbering scheme (Ballesteros and Weinstein, 1995). The numbers above the NK3R_HUMAN receptor gives the sequence number of the positions of the mutations carried out in this study. The amino acid sequences of the human NK$_3$R (accession no. P29371), rat NK$_3$R (accession no. P16177), mouse NK$_3$R (accession no. P47937), gerbil NK$_3$R (accession no. AM157740), human NK$_1$R (accession no. P25103), and human NK$_2$R (accession no. P21452) were retrieved form the Swiss-Prot database.

(Hoffmann et al., 2005). As seen in Table 3, the mutations M346A and S348A led to increases in the K_i values of RO4908594 for displacing of [^{3}H]osanetant by 3.8-fold (P = 0.007) and 5.0-fold (P = 0.0009), respectively. It is noteworthy that the F342A mutant, which had led to complete loss of [^{3}H]Me-talnetant binding affinity and also a decrease in [^{3}H]osanetant affinity (Table 1), displayed a 80-fold (P = 0.0006) higher affinity for RO4908594 in displacing of [^{3}H]-osanetant than the WT (Table 3). Of note is the mutation of Y315F, which increased RO4908594 binding affinity by 2.5-fold (P = 0.02) (Table 3), although it decreased [^{3}H]osanetant binding affinity and had no effect on [^{3}H]Me-talnetant binding affinity (Table 1).

Effect of Mutations on the [MePhe^7]NKB-Evoked Accumulation of [^{3}H]IP. To obtain more information about the NK$_3$R agonist binding pocket, the effects of mutations on NKB-induced formation of [^{3}H]IP were investigated in CHO cells expressing transiently the WT and mutated hNK$_3$Rs. [MePhe^7]NKB (0.1 nM-10 μM) elicited a concentration-dependent increase in the accumulation of [^{3}H]IP in the cells expressing WT and mutated hNK$_3$Rs. The EC$_{50}$, n_H, and relative E_{max} values, calculated from concentration-response curves of [MePhe^7]NKB in the cells expressing WT and mutated receptors, are given in Table 4. The [MePhe^7]NKB showed a lower functional potency (by 918.9-, 14.4-, and 117.1-fold, with statistically significant P < 0.0001) and ef-

TABLE 1

[^{3}H]Me-talnetant and [^{3}H]osanetant binding properties at human wild-type and mutated NK$_3$Rs

Saturation binding isotherms of [^{3}H]Me-talnetant and [^{3}H]osanetant were performed on membrane preparations from HEK293-EBNA cells transiently transfected with the WT and mutated hNK$_3$Rs as described under *Materials and Methods*. The K_d and B_{max} values are mean ± S.E., calculated from three independent experiments (each performed in triplicate). The mutations that affected the binding affinities of [^{3}H]Me-talnetant and [^{3}H]osanetant comparison with the WT are shown in bold. Statistical significance was determined using a two-tailed t test.

hNK$_3$R	Position in the 7TMD	[^{3}H]Me-Talnetant Binding			[^{3}H]Osanetant Binding		
		K_d	K_d (Mutant)/K_d (WT)	B_{max}	K_d	K_d (Mutant)/K_d (WT)	B_{max}
		nM		*pmol/mg protein*	*nM*		*pmol/mg protein*
WT		0.8 ± 0.1		34.3 ± 0.5	0.2 ± 0.0		26.0 ± 0.5
V95A	1.42	**3.2 ± 0.1**	**4.0*****	46.6 ± 6.6	**0.5 ± 0.1**	**2.3***	28.6 ± 2.5
V95L	1.42	1.0 ± 0.1	1.2	36.3 ± 12.1	0.3 ± 0.0	1.7	40.9 ± 2.0
V95I/A99S	1.42, 1.46	**2.4 ± 0.2**	**3.0****	69.7 ± 11.8	**0.7 ± 0.1**	**3.5****	48.3 ± 0.8
M134A	2.53	N.B.	N.B.		N.B.	N.B.	
N138A	2.57	**2.8 ± 0.5**	**3.5****	45.7 ± 10.5	**0.8 ± 0.1**	**3.8***	18.8 ± 0.4
T139A	2.58	2.3 ± 0.6	2.8	56.2 ± 11.6	0.3 ± 0.1	1.6	41.1 ± 2.8
V95L/T139A	1.42, 2.58	1.5 ± 0.2	1.9	59.4 ± 5.9	0.2 ± 0.1	1.1	58.3 ± 4.5
N142A	2.61	**0.1 ± 0.0**	**0.1****	27.6 ± 0.3	N.B.	N.B.	
V169M	3.36	N.B.	N.B.		N.B.	N.B.	
L232A	45.49	1.4 ± 0.3	1.8	30.1 ± 5.6	0.3 ± 0.0	1.4	15.7 ± 1.0
Y315F	6.51	1.3 ± 0.1	1.7	23.3 ± 1.2	**1.8 ± 0.2**	**9.0*****	18.6 ± 0.7
S341A	7.38	1.0 ± 0.0	1.3	47.2 ± 2.5	0.1 ± 0.0	0.7	34.2 ± 0.5
F342A	7.39	N.B.	N.B.		**3.4 ± 0.7**	**17.0****	16.6 ± 2.5
F342M	7.39	N.B.	N.B.		N.B.	N.B.	
S341I/F342M	7.38, 7.39	N.B.	N.B.		N.B.	N.B.	
M346A	7.43	**2.0 ± 0.1**	**2.5****	55.2 ± 2.6	0.2 ± 0.0	1.1	36.1 ± 0.9
S348A	7.45	1.3 ± 0.1	1.7	31.9 ± 1.0	0.3 ± 0.1	1.4	15.2 ± 0.6

N.B., no binding.
* P < 0.05.
** P < 0.01.
*** P < 0.001.

TABLE 2

Effects of the mutations on [^{3}H]Me-talnetant displacement by [MePhe^7]NKB, osanetant, and SB222200 in the membrane preparations from HEK293-EBNA cells transiently expressing WT and mutated hNK$_3$Rs

K_i and n_H values for [^{3}H]Me-talnetant binding inhibition by [MePhe^7]NKB, osanetant, or SB222200 were calculated as described under *Materials and Methods*. Values are mean ± S.E. of the K_i calculated from three independent experiments, each performed in duplicate. The mutations that affected the affinity constants of [MePhe^7]NKB, osanetant, and SB222200 in comparison with WT are shown in boldface type. Statistical significance was determined using a two-tailed t test.

| hNK$_3$R	[MePhe^7]NKB			Osanetant			SB222200		
	K_i	K_i (Mutant)/K_i (WT)	n_H	K_i	K_i (Mutant)/K_i (WT)	n_H	K_i	K_i (Mutant)/K_i (WT)	n_H
	nM			*nM*			*nM*		
WT	14.7 ± 2.8		0.6 ± 0.0	1.0 ± 0.3		1.1 ± 0.2	5.4 ± 0.5		0.9 ± 0.0
V95A	19.4 ± 4.1	1.3	0.9 ± 0.1	**14.0 ± 3.9**	**13.6***	0.6 ± 0.1	**27.1 ± 5.4**	**5.0***	0.7 ± 0.1
V95L	7.9 ± 0.9	0.5	0.7 ± 0.1	1.8 ± 0.4	1.8	1.0 ± 0.1	4.6 ± 0.2	0.9	0.9 ± 0.0
V95I/A99S	12.9 ± 0.6	0.9	0.8 ± 0.1	1.7 ± 0.4	1.7	0.8 ± 0.1	12.5 ± 5.5	2.3	0.8 ± 0.2
N138A	**875.0 ± 103.0**	**59.4*****	0.9 ± 0.1	**11.5 ± 0.7**	**11.2*****	0.9 ± 0.3	**21.0 ± 4.9**	**3.9***	0.8 ± 0.0
T139A	24.7 ± 8.8	1.7	0.9 ± 0.1	0.9 ± 0.7	0.9	0.6 ± 0.2	15.7 ± 2.1	2.9	0.9 ± 0.0
V95L/T139A	7.8 ± 2.9	0.5	0.6 ± 0.1	1.7 ± 0.1	1.6	1.0 ± 0.0	8.9 ± 0.8	1.7	1.0 ± 0.0
N142A	>10,000			**128.0 ± 4.9**	**124.3*****	1.1 ± 0.1	**0.01 ± 0.001**	**0.002*****	0.5 ± 0.0
L232A	**147.0 ± 7.8**	**10.0*****	0.8 ± 0.1	1.5 ± 0.6	1.5	0.4 ± 0.0	15.0 ± 3.8	2.8	0.8 ± 0.0
Y315F	**90.8 ± 18.5**	**6.2***	1.1 ± 0.1	**12.6 ± 1.8**	**12.2****	1.1 ± 0.3	8.0 ± 0.9	1.5	0.9 ± 0.1
S341A	17.1 ± 3.7	1.2	0.7 ± 0.1	1.2 ± 0.3	1.2	1.0 ± 0.2	5.8 ± 0.5	1.1	0.9 ± 0.0
M346A	**207.0 ± 31.8**	**14.1****	1.0 ± 0.1	0.9 ± 0.4	0.9	0.7 ± 0.0	10.6 ± 0.6	2.0	0.7 ± 0.0
S348A	27.6 ± 4.4	1.9	0.8 ± 0.1	2.4 ± 1.0	2.3	0.5 ± 0.1	9.2 ± 0.2	1.7	0.9 ± 0.1

* P < 0.05.
** P < 0.01.
*** P < 0.001.

ficacy (relative E_{max} of 45, 66, and 80%) at the mutants N138A, N142A, and F342A, respectively, in comparison with the WT. The mutation M346A caused a 21.6-fold ($P < 0.0001$) decrease in potency of [MePhe[7]]NKB without any effect on its efficacy. The mutants L232A, Y315F, F342M, and S341I/F342M exhibited moderate increases in the [MePhe[7]]NKB EC_{50} values (5.3-, 5.2- 9.0-, and 9.0-fold, respectively, with statistically significant $P < 0.0001$) compared with WT. Although the same mutations have been observed to affect both the functional potency (Table 4) and affinity constant (Table 2) of [MePhe[7]]NKB, there were differences in the extent of the effect in two assays [e.g., the mutation N142A that abolished the affinity of [MePhe[7]]NKB in competition binding (K_i >10,000 nM) decreased [MePhe[7]]NKB potency by only 14.4-fold in functional assay, and vice versa, the mutation N138A, which had a dramatic effect on NKB functional potency (EC_{50} of 1020 nM versus 1.1 nM for WT), increased NKB K_i value by 59-fold in competition binding].

Effect of Mutations on the Schild analyses of Me-Talnetant and Osanetant as Measured by [MePhe[7]]-

NKB-Induced [^{3}H]IP Accumulation Assay. To characterize the effects of mutations on antagonism potency and the inhibition mode of Me-talnetant and osanetant, the concentration-response curves (CRCs) for [^{3}H]IP formation stimulated by [MePhe[7]]NKB have been measured in the presence of 0, 10, 30, and 100 nM Me-talnetant or 0, 30, 100, and 300 nM osanetant in CHO cells expressing transiently the WT and mutated hNK$_3$Rs. As seen in Fig. 5, A and C, both Me-talnetant and osanetant behave as a competitive antagonist at WT hNK$_3$R, shifting the NKB CRC to the right without changing its maximal response. Me-talnetant displayed an apparent antagonist potency (pA_2) of 8.14 (or K_b^a = 7.2 nM) and a Schild slope of 0.81 (Fig. 5B), which is in good agreement with its affinity constant and is consistent with a competitive mode of action. However, osanetant had an apparent antagonist potency (pA_2) of 7.47 (or K_b^a = 33.9 nM), which is almost 2 log values lower than its binding constant (pK_i = 9.6), and a Schild slope of 1.80, which has deviated from simple competitive antagonism with unit slope (Fig. 5D).
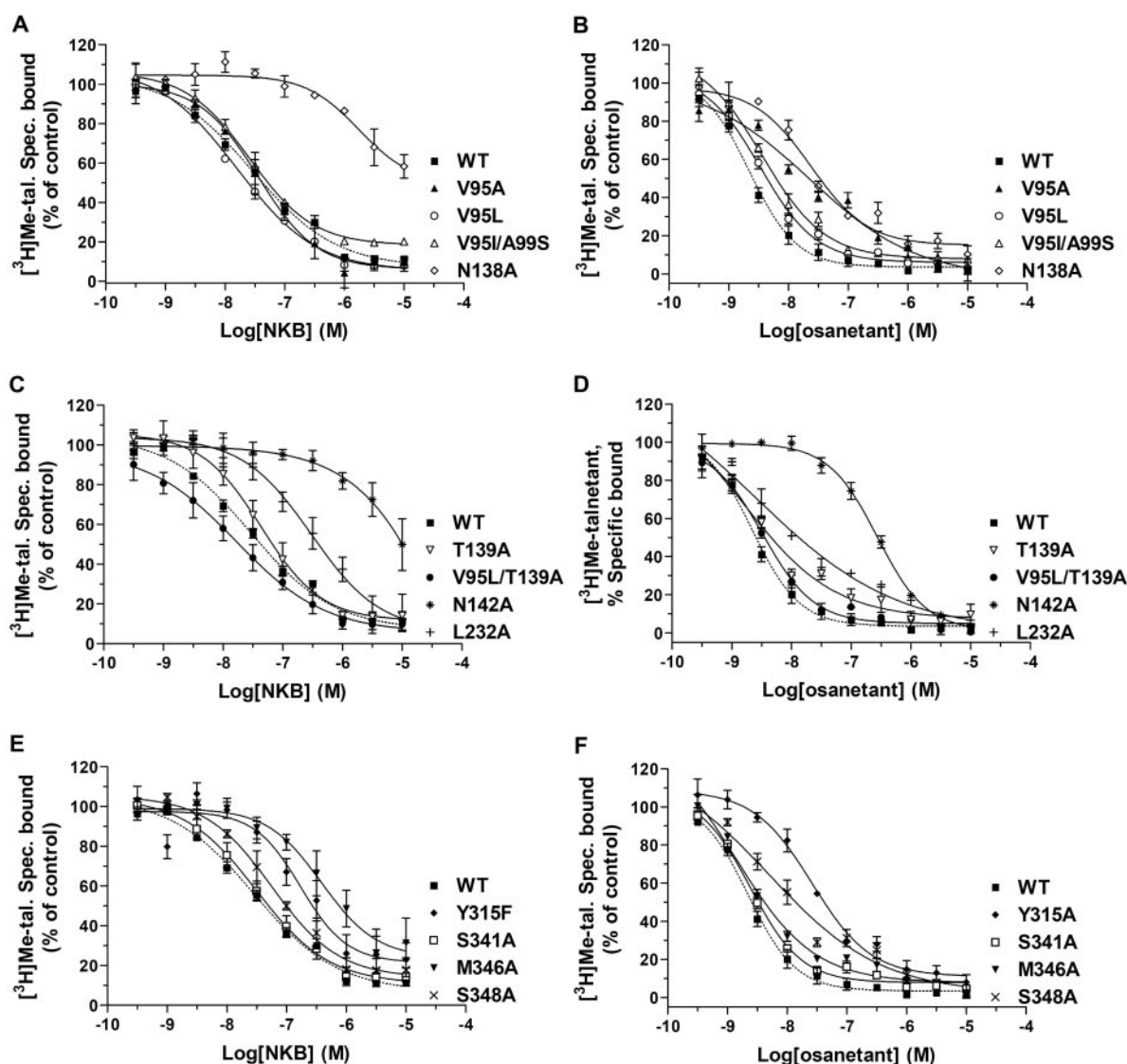
Fig. 4. Effects of the mutations on the competition binding of [MePhe[7]]NKB and osanetant in membrane preparations from HEK293-EBNA cells transiently expressing WT and mutated NK$_3$Rs. The [^{3}H]Me-talnetant at a concentration equal to its K_d value was used in these competition binding experiments. Each data point is mean ± S.E. (bars) of three individual experiments performed in duplicate.

As observed above (Table 4), NKB has kept its potency on most of the mutated receptors except for the mutant N138A, where it was inactive. Therefore, the antagonism potency of Me-talnetant and osanetant were determined at the mutated receptors using Schild analyses. The apparent antagonist potency (pA_2) and Schild slope values of Me-talnetant and osanetant at the mutated hNK_3Rs are given in the Table 5. In general, there was a good agreement between the effects of mutations on binding affinity and functional potency results for both antagonists (Tables 1 and 5). In cells expressing four mutants, M134A, V169M, F342M, and S341I/F342M, which did not bind [³H]Me-talnetant and [³H]osanetant, both antagonists were inactive and they were not able to produce

right shift of NKB CRC. In good agreement with the binding experiments, the mutant N142A, which caused an increase in binding affinity of Me-talnetant, also resulted in an increase of Me-talnetant antagonism potency, whereas the same mutation abolished the osanetant affinity and potency. The mutation F342A, which led to the loss of Me-talnetant affinity, similarly resulted in a loss of antagonism potency. In osanetant, the mutant F342A decreased the antagonist potency, a result consistent with the 17-fold decrease of osanetant binding affinity. Among the mutated receptors, the mutants T139A and M346A exhibited the NKB CRC in presence of increasing fixed concentrations of osanetant that shifted to the right with a concomitant decrease in NKB maximal response, a fact inconsistent with a simple competitive mode of antagonism (Fig. 5, E and F; Table 5).

Binding Kinetics of [³H]Me-Talnetant and [³H]Osanetant to hNK_3R WT and Mutants T139A and M346A. Binding of [³H]Me-talnetant and [³H] osanetant to the WT receptor was rapid, with half-maximal binding occurring at 1.4 and 4 min and reaching equilibrium within 15 and 30 min, respectively. The data from both antagonists were fit to a one-phase exponential model with the association rate constants of 0.34 ± 0.06 $nM^{-1}min^{-1}$ and 0.33 ± 0.04 $nM^{-1}min^{-1}$, respectively (Fig. 6A; Table 6). The association bindings of [³H]osanetant to the mutants T139A and M346A were similar to the WT, with half-maximal binding, $t_{1/2}$ values of 4.6 and 5 min, respectively (Fig. 6A; Table 6).

The dissociation rates for [³H]Me-talnetant and [³H]osanetant binding to the WT receptor was determined by the addition of an excess amount of SB222200 after equilibrium (30 min and 1 h, respectively) was reached. The reversal of binding for both antagonists was complete, with $t_{1/2}$ values of 4.6 and 10 min, respectively (Fig. 6B; Table 6). The rates of [³H]osanetant dissociation from the mutants T139A and M346A were decreased compared with the WT, with half-reversal binding occurring, $t_{1/2}$ values of 21 and 18 min, respectively (Fig. 6B; Table 6). The calculations of the appar-

TABLE 3
Effects of the mutations on [³H]osanetant displacement by RO4908594 in the membrane preparations from HEK293-EBNA cells transiently expressing WT and mutated hNK_3Rs

K_i and n_H values for [³H]osanetant binding inhibition by RO4908594 calculated as described under *Materials and Methods*. Values are mean ± S.E. of the K_i calculated from three independent experiments, each performed in duplicate. The mutations that affected the affinity constants of RO4908594 in comparison with WT are shown in bold. Statistical significance was determined using a two-tailed t test.

hNK_3R	RO4908594		
	K_i	K_i (Mutant)/K_i (WT)	n_H
	nM		
WT	1.6 ± 0.1		1.1 ± 0.1
V95A	1.6 ± 0.4	1.0	0.9 ± 0.1
V95L	3.5 ± 0.1	2.2	1.0 ± 0.0
V95I/A99S	4.2 ± 0.8	2.6	1.1 ± 0.1
N138A	4.0 ± 0.7	2.5	1.2 ± 0.1
T139A	2.9 ± 0.5	1.8	1.0 ± 0.1
V95L/T139A	4.9 ± 0.5	3.1	1.1 ± 0.0
L232A	1.6 ± 0.2	1.0	1.1 ± 0.0
Y315F	**0.6 ± 0.04**	**0.4***	1.6 ± 0.1
S341A	2.0 ± 0.2	1.3	1.3 ± 0.3
F342A	**0.02 ± 0.0**	**0.01***	0.8 ± 0.2
M346A	**6.0 ± 0.3**	**3.8***	1.1 ± 0.1
S348A	**8.0 ± 0.1**	**5.0***	1.1 ± 0.1

* $P < 0.05$.
** $P < 0.01$.
*** $P < 0.001$.

TABLE 4
Effect of mutations on the [MePhe⁷]NKB-evoked accumulation of [³H]IP. EC_{50}, n_H, and E_{max} values for the NKB-induced formation of [³H]IP in CHO cells expressing transiently the WT and mutated hNK_3Rs

The data are mean ± S.E. of eight concentration-response measurements (each performed in duplicate) from four independent transfections. The mutations that affected the potency of [MePhe⁷]NKB in comparison with WT are shown in bold. Statistical significance was determined using a two-tailed t test.

hNK_3R	Position in the 7TMD	[MePhe⁷]NKB			
		EC_{50}	EC_{50} (Mutant)/EC_{50} (WT)	n_H	Relative E_{max}
		nM			
WT		1.1 ± 0.0		1.5 ± 0.1	100
V95A	1.42	1.6 ± 0.4	1.5	1.6 ± 0.2	113.5 ± 10.2
V95L	1.42	2.3 ± 0.4	2.1	2.0 ± 0.2	86.5 ± 14.5
V95I/A99S	1.42, 1.46	1.4 ± 0.2	1.3	2.0 ± 0.4	105.1 ± 6.8
M134A	2.53	1.8 ± 0.2	1.6	2.1 ± 0.2	110.0 ± 6.4
N138A	2.57	**1020.0 ± 43.9**	**918.9***	1.6 ± 0.3	45.2 ± 13.0
T139A	2.58	2.8 ± 0.8	2.5	1.4 ± 0.1	90.2 ± 32.2
V95L/T139A	1.42, 2.58	5.2 ± 0.2	4.7	1.6 ± 0.1	120.3 ± 6.0
N142A	2.61	**16.0 ± 0.8**	**14.4***	1.1 ± 0.1	66.1 ± 17.9
V169M	3.36	4.6 ± 1.5	4.1	1.0 ± 0.2	104.0 ± 13.4
L232A	45.49	**5.9 ± 0.4**	**5.3***	1.1 ± 0.1	99.8 ± 4.0
Y315F	6.51	**5.8 ± 0.9**	**5.2***	0.9 ± 0.2	71.8 ± 15.2
S341A	7.38	2.8 ± 0.6	2.5	1.9 ± 0.3	106.5 ± 11.4
F342A	7.39	**130.0 ± 11.0**	**117.1***	1.2 ± 0.3	80.5 ± 5.7
F342M	7.39	**10.0 ± 1.4**	**9.0***	0.9 ± 0.1	72.9 ± 13.9
S341I/F342M	7.38, 7.39	**10.0 ± 2.2**	**9.0***	0.8 ± 0.1	102.9 ± 12.1
M346A	7.43	**24.0 ± 2.9**	**21.6***	0.9 ± 0.2	113.0 ± 4.3
S348A	7.45	3.7 ± 1.0	3.3	1.2 ± 0.1	103.3 ± 7.8

*** $P < 0.001$.

ent K_d values derived from the kinetic experiments are given in Table 6. The apparent K_d value of [³H]Me-talnetant (0.44 ± 0.15 nM) was lower than that of equilibrium K_d value (0.8 ± 0.1 nM). [³H]osanetant had an apparent K_d value of 0.22 ± 0.06 nM at WT receptor, which is in good agreement with the equilibrium K_d value (0.2 ± 0.0 nM). However, the apparent K_d values of [³H]osanetant at the mutants T139A and M346A (0.12 ± 0.01 and 0.11 ± 0.01 nM) were lower that those of equilibrium K_d values (0.3 ± 0.1 and 0.2 ± 0.0 nM, respectively).

Docking of Me-Talnetant, Osanetant, and RO4908594 onto the NK₃R-7TMD Binding Cavity. To visualize the mutation data, a 3D model of the hNK₃R-7TMD using the atomic coordinates of bovine rhodopsin (Protein Data Bank reference code 1f88) was constructed. Figure 7A shows the residues in the TM region mutated in this study, and it suggests possible binding modes for Me-talnetant and osanetant. On the basis of a ligand-based alignment of osanetant and RO4908594, which was generated by comparing the observed SAR of the two chemical classes, a docking mode was
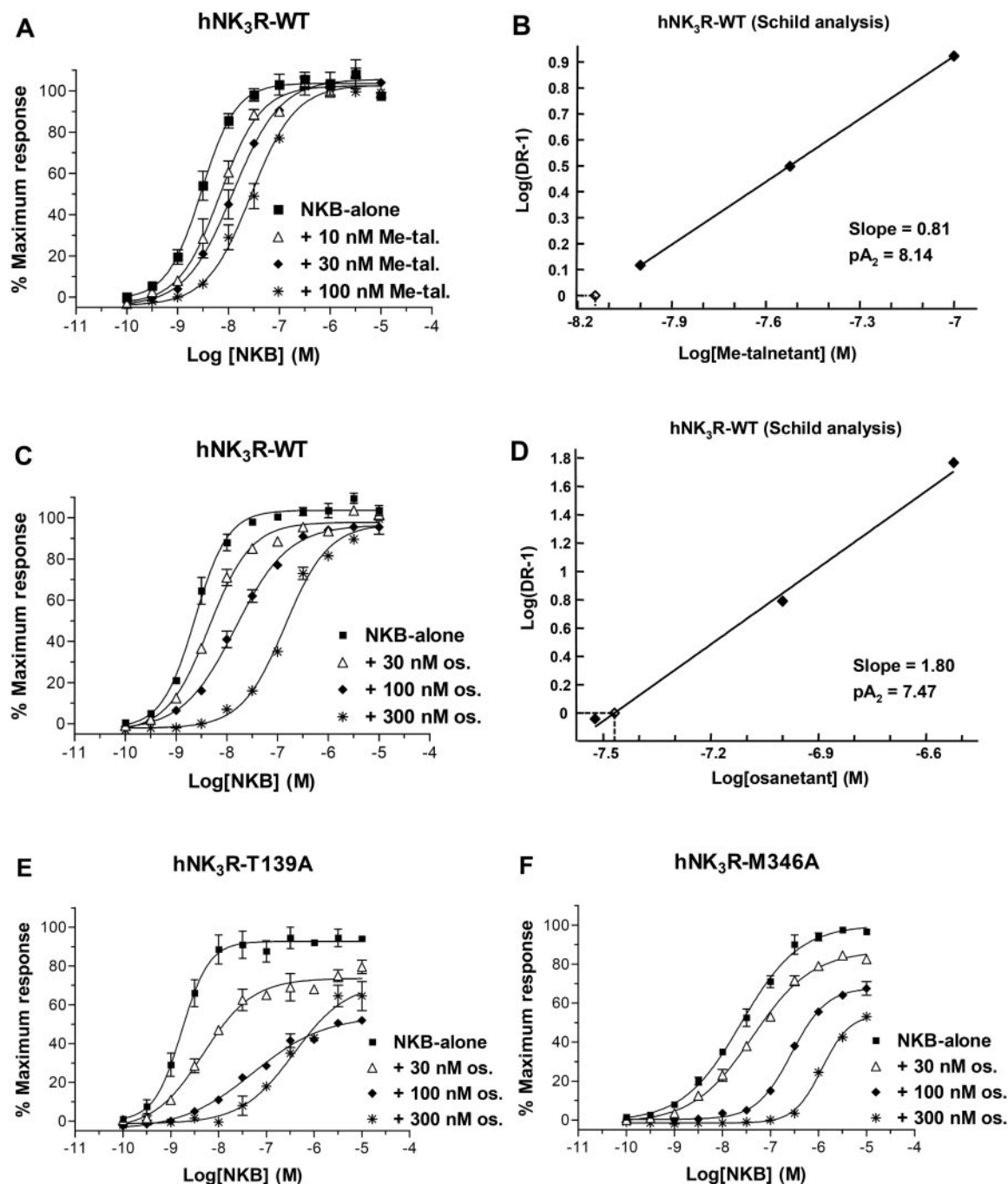
Fig. 5. Schild plot analyses for antagonism of [MePhe⁷]NKB-induced accumulation of [³H]IP by Me-talnetant and osanetant. CRCs for [³H]IP formation stimulated by [MePhe⁷]NKB in the absence and presence of various concentrations of Me-talnetant (A) and osanetant (C, E, and F) in CHO cells expressing transiently the hNK₃R WT, T139A, and M346A. Schild plots for antagonism by Me-talnetant (B) and osanetant (D). The EC₅₀ and EC′₅₀ values, which derived from NKB CRCs in the absence and presence of increasing fixed concentrations of Me-talnetant or osanetant (A and C), were used to calculate the dose ratios (DR = EC′₅₀/EC₅₀) and plotted according to Schild regression in B and D. Each curve represents the mean of eight concentration-response measurements from a minimum of two independent transfections.

proposed for RO4908594 (Fig. 7B). Looking at the predicted docking mode of RO4908594, one recognizes at once that the 4-phenyl substituent seems to be too close to Phe342, causing a clash. Therefore, the mutation of this residue to a smaller one is expected to result in a significant affinity increase.

The proposed docking poses (Fig. 7, A and B) of Me-talnetant, osanetant, and RO4908594 are in good agreement with the results of the mutation studies. It is important to note that it is often difficult to decide whether an observed effect of a mutation onto binding affinity of a ligand goes back to a direct interaction between this residue and the ligand or whether the mutation leads to conformational changes of the binding site. This is especially true for mutations that lead to a loss of affinity for all tested ligands. If a ligand is not affected by a mutation, one can assume that the residue most likely does not affect the conformation of the binding site. Consequently, ligands that are affected in their affinity by this mutation most likely form a direct interaction with the residue. In this context, two examples of mutations (V95A and N138A) that affected both the binding of Me-talnetant and osanetant, but not RO4908594, were observed. Thus, there is a strong suggestion of direct interactions. Moreover, when a mutation results in a gain of affinity for a ligand, as predicted on the basis the proposed docking pose, one can also be confident that this goes back onto a direct (negative) interaction because the chance that a gain of affinity is caused by conformational changes is rather small. Here, two mutations led to such a gain of affinity for RO4908594 (F342A and Y315F). Based on the predicted docking pose, this gain in affinity was expected in both cases, and it is most likely caused by direct interactions (anticipated relief of steric hindrance or removal of polar groups without binding partner) and not by indirect effects due to conformational changes.

Discussion

Here, we have determined the likely binding pockets of Me-talnetant and osanetant using site-directed mutagenesis and rhodopsin-based modeling of hNK$_3$R-7TMD. These mutated hNK$_3$Rs also made it possible to probe the NKB binding pocket on the basis of [MePhe^7]NKB-evoked accumulation of [^{3}H]IP and competitive binding with [^{3}H]Me-talnetant. The residues Asn138$^{2.57}$, Asn142$^{2.61}$, Leu232$^{45.49}$, Tyr315$^{6.51}$, Phe342$^{7.39}$, and Met346$^{7.43}$ were found to be crucial for the NKB binding site.

In the TM1 region, the V95$^{1.42}$A mutation had a significant effect onto the binding of Me-talnetant and a lesser one on osanetant binding. This is in agreement with the proposed docking mode according to which the benzylamine substructure of Me-talnetant reaches deeply into the pocket formed by the TM1, -2, and -7, whereas osanetant does not fill this region of space (Fig. 7A). The aromatic ring of this Me-talnetant chain is thus located closely to Val95$^{1.42}$. Because this mutation does not affect the binding of RO4908594, it is assumed that Me-talnetant indeed forms a direct interaction with Val95$^{1.42}$. The position 95 is not conserved in the hNK$_1$R and hNK$_2$R (Fig. 3). The incorporation of a leucine (V95$^{1.42}$L) as in hNK$_2$R did not affect either of the ligands. Although Val95$^{1.42}$ obviously forms a hydrophobic interaction with Me-talnetant that contributes to the binding affinity, there is still enough space to incorporate the larger leucine residue. The double-mutant V95$^{1.42}$L/T139$^{2.58}$A incorporating two residues of the hNK$_2$R located closely together in 3D also did not influence the binding affinities. Because the leucine residue also is tolerated, we did not incorporate the isoleucine residue of hNK$_1$R as a single point-mutation, assuming that this residue is tolerated, too.

In the TM2 region, the mutant M134$^{2.53}$A did not bind either Me-talnetant or osanetant. For osanetant, this result was expected because Met134$^{2.53}$ had previously been shown to be an important factor for species selectivity (Wu et al., 1994). According to the proposed docking modes, both ligands indeed form direct interactions with Met134$^{2.53}$, Me-talnetant via the ethyl side chain, osanetant via its benzoyl chain. However, one cannot rule out that, because of this mutation, a conformation change of the binding site might also lead indirectly to the observed loss of affinity of both ligands. Asn138$^{2.57}$ is located one turn above Met134$^{2.53}$. Its mutation

TABLE 5
Schild constants for antagonism of [MePhe^7]NKB-induced accumulation of [^{3}H]IP by Me-talnetant and osanetant in CHO cells expressing transiently the WT and mutated hNK$_3$Rs

The pA_2 and Schild slope values of Me-talnetant and osanetant at the WT and mutated hNK$_3$Rs were determined from NKB CRCs in the absence and presence of various concentrations of antagonist and Schild plot analyses shown in Fig. 5.

| hNK$_3$R	Position in the 7TMD	Me-Talnetant		Osanetant	
		pA_2	Schild Slope	pA_2	Schild Slope
WT		8.14	0.81	7.47	1.80
V95A	1.42	7.88	1.28	7.46	1.85
V95L	1.42	7.59	1.70	7.24	1.70
V95I/A99S	1.42, 1.46	7.53	1.37	7.05	1.43
M134A	2.53	Inactive		Inactive	
N138A	2.57	NKB inactive		NKB inactive	
T139A	2.58	8.45	0.86	7.66	2.11
V95L/T139A	1.42, 2.58	7.52	1.04	7.18	1.85
N142A	2.61	8.76	1.15	Inactive	
V169M	3.36	Inactive		Inactive	
L232A	45.49	8.19	1.20	7.42	1.82
Y315F	6.51	8.05	1.50	7.08	0.83
S341A	7.38	7.79	1.64	7.28	1.56
F342A	7.39	Inactive		6.86	0.86
F342M	7.39	Inactive		Inactive	
S341I/F342M	7.38, 7.39	Inactive		Inactive	
M346A	7.43	8.07	1.12	7.48	1.83
S348A	7.45	8.08	1.19	7.46	1.79

to alanine led for both ligands to a 3.5× loss of affinity, but it did not affect RO4908594 binding. Thus, Me-talnetant and osanetant probably form a direct interaction with Asn138[2.57] that is lost upon mutation to alanine. The result of the mutation N142[2.61]A is surprising. Although binding of osanetant is completely lost, Me-talnetant binding is significantly increased. Because Asn142[2.61] is located closely to several other polar residues, it is most likely part of a larger hydrogen-bonding network, and the observed effect is perhaps an indirect effect.

In the TM3, -6, and -7 regions, the mutation V169[3.36]M led for both ligands to a complete loss of affinity. This mutation incorporates the residue of NK$_2$R into the NK$_3$R. Me-talnetant and osanetant have NK$_3$R selectivity; i.e., they are more selective for NK$_3$R because they have increased affinity for this receptor. It is interesting to note that in the 3D model, the residue Val169[3.36] is located in proximity to Trp263[6.48] in the TM6 helix; thus, it is likely to be part of the intramolecular TM network involved in receptor activation, as shown previously for rhodopsin (Trp265[6.48]) and other class A GPCRs (Sheikh et al., 1996; Ballesteros et al., 2001). Val169[3.36] is located too far away from the two compounds for

Fig. 6. Time course for the association (A) and dissociation (B) of [^{3}H]Me-talnetant binding to hNK$_3$R WT membranes and [^{3}H]osanetant binding to the hNK$_3$R WT, T139A, and M346A membranes. Each data point is mean ± S.E. (bars) of three individual experiments performed in quadruplet.

a direct interaction, and one has to assume that the observed loss of affinity for Me-talnetant and osanetant is due to conformation changes caused by the mutation to methionine. The mutation of Tyr315[6.51] to its corresponding residue in the NK$_1$R (Phe) affected only osanetant binding, which was partially lost. This shows that Tyr315[6.51] is one of the factors of NK$_1$R selectivity of osanetant, which binds to hNK$_1$R with K_i of 744 nM, whereas the K_i of talnetant at hNK$_1$R is >100,000 nM (Sarau et al., 1997). Because this mutation did not affect Me-talnetant binding, in osanetant the affinity loss is presumably due to the loss of a direct interaction. This result is in agreement with the proposed docking pose that allows the phenolic OH of Tyr315[6.51] to form a hydrogen bond with the piperazine ring of osanetant, whereas Me-talnetant can interact only with the aromatic ring but not the OH group (Fig. 7A). RO4908594 cannot interact with the OH group either, but opposite to Me-talnetant it comes close to this OH moiety, which causes an unfavorable situation. This explains why the Y315F mutant results in an affinity increase of this compound. Mutation of Phe342[7.39] to methionine, the corresponding residue in NK$_1$R, led to a complete loss of affinity for both ligands that make hydrophobic interactions with this residue: Me-talnetant via its 2-phenyl ring and osanetant via its dichloro-substituted phenyl ring. Mutation of Phe342[7.39] to alanine led to a complete loss of affinity for Me-talnetant, to a 17-fold loss of affinity for osanetant, but to a significant affinity increase for RO4908594. These results are in agreement with its proposed docking mode according to which the 4-phenyl substituent of RO4908594 clashes into the large phenylalanine at this position. Again, the observed affinity increase for RO4908594 strengthened the hypothesis of Me-talnetant and osanetant forming direct interactions with the mutated residue. A different behavior of Me-talnetant and osanetant is observed with the M346[7.43]A mutant that does not affect osanetant binding but leads to a significant loss of Me-talnetant affinity. According to the docking mode, Me-talnetant can indeed form a hydrophobic interaction with Met346, whereas osanetant is located too far from this residue. RO4908594 can also interact with Met346; thus, the observed partial loss of affinity with the M346A mutant is in agreement with the docking hypothesis of this compound.

The functional potencies of Me-talnetant and osanetant on mutated receptors as determined by Schild plot analyses are mostly in agreement with the binding affinities. Although the Schild slope of osanetant at WT and some mutated receptors exhibited deviation from simple competitive antagonism with unit slope, in general, osanetant behaved competitively at the mutated receptors except for the mutants
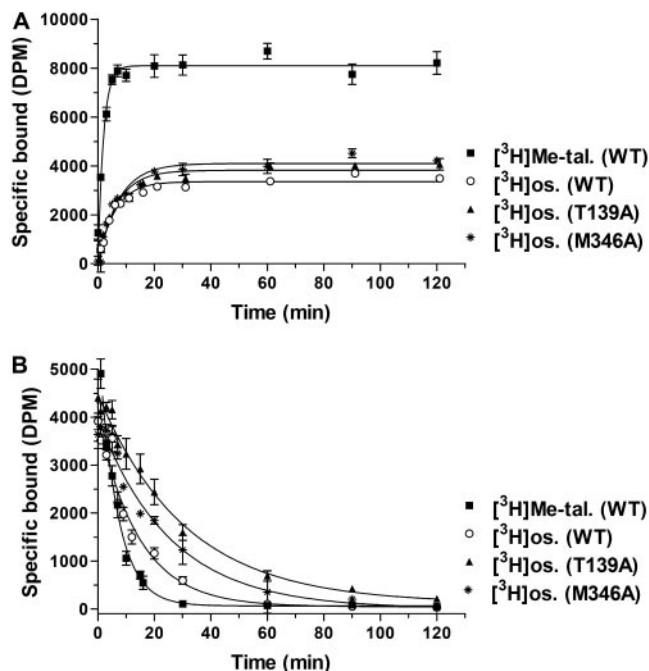
TABLE 6

$K_i$netic parameters for association and dissociation of ^{3}H]Me-talnetant in hNK$_3$R WT membranes and of [^{3}H]osanetant in the hNK$_3$R WT, T139A, and M346A membranes

The K_{ob}, K_{off}, K_{on}, $t_{1/2}$, and K_d values are mean ± S.E., calculated from three independent experiments (each performed in quadruplet) as described under *Materials and Methods*.

Compound	hNK$_3$R	Association Kinetic			Dissociation Kinetic		Apparent K_d
		K_{ob}	K_{on}	$t_{1/2}$	K_{off}	$t_{1/2}$	
		min^{-1}	*nM*$^{-1}$ *min*$^{-1}$	*min*	*min*$^{-1}$	*min*	*nM*
[^{3}H]Me-talnetant	WT	0.49 ± 0.04	0.34 ± 0.06	1.41 ± 0.16	0.15 ± 0.03	4.56 ± 0.52	0.44 ± 0.15
[^{3}H]Osanetant	WT	0.17 ± 0.02	0.33 ± 0.04	4.01 ± 0.73	0.07 ± 0.01	10.10 ± 1.07	0.22 ± 0.06
	T139A	0.15 ± 0.01	0.29 ± 0.07	4.60 ± 0.31	0.03 ± 0.01	21.43 ± 2.4	0.12 ± 0.01
	M346A	0.14 ± 0.01	0.29 ± 0.06	5.04 ± 0.27	0.04 ± 0.01	17.72 ± 1.93	0.11 ± 0.01

T139A and M346A, which displayed abnormal Schild plots. Our binding kinetics showed that osanetant had a slower dissociation rate on these mutants than that of WT; this might explain the abnormal Schild analyses observed in the [MePhe[7]]NKB-evoked accumulation of [^{3}H]IP assay.

These observations show that the binding pockets of Me-talnetant and osanetant are overlapping, but not identical. Although Me-talnetant binding is more influenced by residues on TM1 and -7, osanetant binding is affected by the mutation Y315[6.51]F. This is in agreement with the proposed docking modes where Me-talnetant reaches deeply into the pocket formed by TM1, -2, and -7, whereas osanetant fills the pocket TM3, -5, and -6 with its phenyl-piperidine fragment (Fig. 7A).

When the critical residues involved in the NKB-, Me-talnetant-, and osanetant binding site of hNK$_3$R were compared with those of reported ligand recognition sites of other neuropeptide GPCRs, a striking conservation was observed in the TM helix position of many critical residues among NK$_1$R, NK$_2$R, NK$_3$R, V$_{1a}$R, and V$_{1b}$R (Table 7). The mutations N138[2.57]A N142[2.61]A of hNK$_3$R that resulted in large decreases of NKB potency and affinity are of special interest, because in hNK$_1$R (Asn85[2.57] and Asn89[2.61]) and hNK$_2$R (Asn86[2.57] and Asn90[2.61]), the equivalent residues were found to be involved in SP and NKA binding sites (Huang et

al., 1994, 1995; Labrou et al., 2001). Met346[7.43] that corresponds to Met297[7.43] of hNK$_2$R was identified to play a role in NKB binding site; it is equivalent to the retinal binding residue Lys296[7.43] of rhodopsin. Furthermore, Labrou et al. (2001) have demonstrated that NKA forms an extended loop-like conformation, in which the C-terminal residues Leu9 and Met10 come into proximity of Met297[7.43] (a deeply buried residue in TM cavity), and Phe6 is close to Tyr266[6.51] and Tyr270[6.55] of hNK$_2$R. Their model also suggested that the residue Asn86[2.57] may not participate in direct interaction with NKA, but nevertheless influence local conformations around Met297[7.43]. Because of a high degree of conservation between the residues involved in NKA and NKB binding sites (Table 7), it is tempting to speculate that NKA and NKB operate with a similar molecular mechanism. There is a high homology between NK$_3$R and V$_1$R, where the ligands all probe similar helix positions in the 7TM (Table 7) (Mouillac et al., 1995; Tahtaoui et al., 2003; Derick et al., 2004). It is noteworthy that the TM helix position 2.61 (located at the rim of 7TM cavity) has similar contact sites with the SP, NKA, NKB, and AVP peptide ligands. Of note are also the TM helix positions 3.36, 6.51, 7.43 (all located deep in TM cavity), and 7.39 (at the top of TM cavity): the residues occupying these helix positions are the most frequently involved in interaction with the diverse ligands of the class A
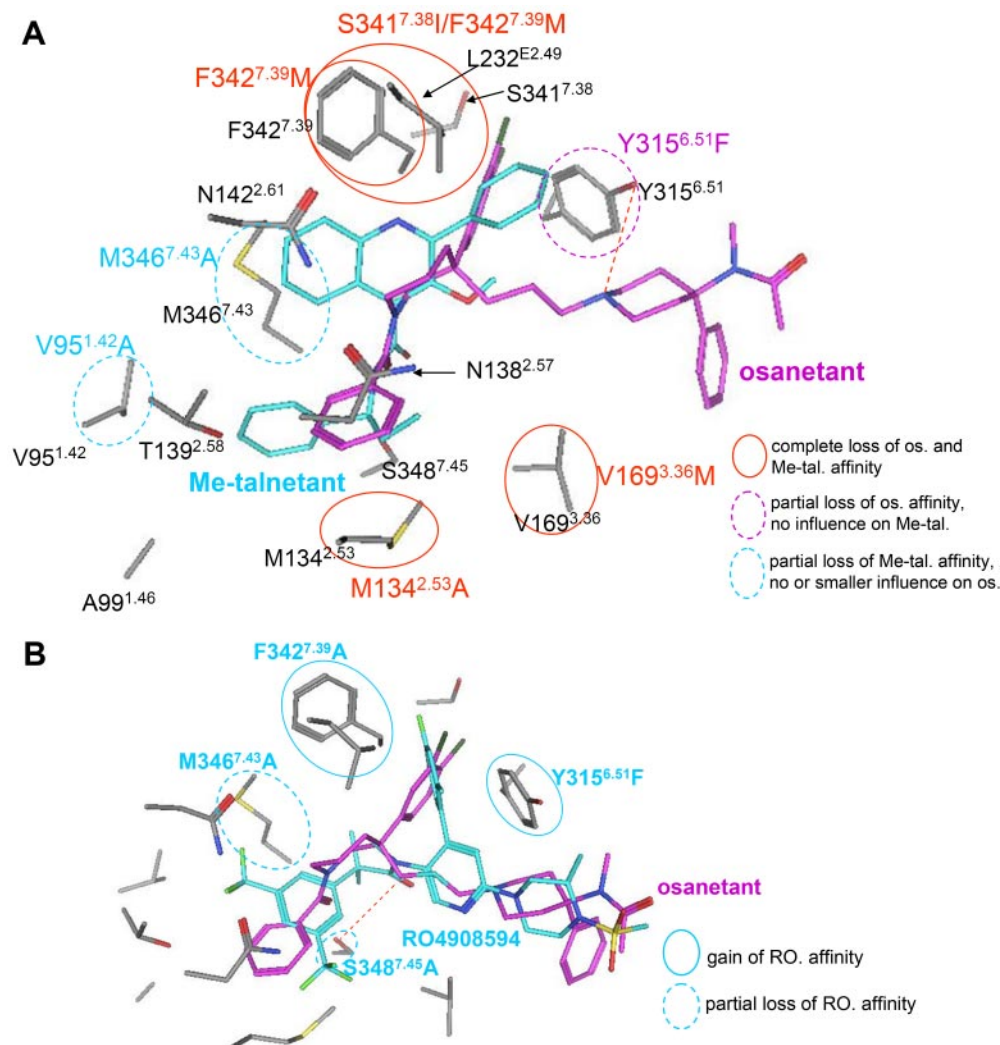
Fig. 7. Proposed docking modes of Me-talnetant and osanetant (A) and comparison with RO4908594 (B). Shown are only the residues that were mutated in this study. The carbon atoms of Me-talnetant and RO4908594 are shown in cyan, those of osanetant in magenta, and protein carbon atoms are in gray. Highlighted in color in A are those mutations that either led to a complete loss of affinity for both Me-talnetant and osanetant (red) or that influenced mainly only one of the two antagonists (magenta, influence on osanetant; cyan, influence on Me-talnetant). Highlighted in cyan in B are those mutations that either led to gain of or partial loss of RO4908594 binding affinity in [^{3}H]osanetant competition binding. Possible hydrogen bond interactions between the piperazine nitrogen of osanetant and the phenolic OH group of Tyr315[6.51] in A and Ser348[7.45] with RO4908594 in B are visualized by red dotted lines.

TABLE 7
Comparison of binding pockets of neurokinin, bradykinin, and vasopressin

The key amino acids located at helix positions in the Ballesteros numbering (Ballesteros and Weinstein, 1995) that have been implicated in the peptide agonist and selective nonpeptide antagonist binding pockets were compared among hNK$_1$R, hNK$_2$R, hNK$_3$R, bradykinin B2 receptor, hV$_{1a}$R, and hV$_{1b}$R. The hNK$_3$R data are from current study

Position in the 7TMD	hNK$_1$R SP[a]	hNK$_2$R NKA[b]	hNK$_2$R Saredutant[c]	hNK$_2$R MEM13510[d]	hNK$_3$R NKB	hNK$_3$R Me-Talnetant	hNK$_3$R Osanetant	Human Bradykinin B2 Receptor FR173657[e]	hV$_{1a}$R AVP[f]	hV$_{1a}$R SR49059[g]	hV$_{1b}$R AVP[f]	hV$_{1b}$R SR149415[h]
2.57	Asn85	Asn86			Asn138							
2.61	Asn89	Asn90			Asn142		Asn142		Gln108		Gln91	
3.36						Val169	Val169		Met135	Met135	Met118	Met118
6.51		Tyr266	Tyr266		Tyr315	Tyr315	Tyr315		Phe307	Phe307	Phe297	Phe297
7.39		Phe293		Phe293	Phe342	Phe342	Phe342			Ala334[i]	Met324	Met324
7.43		Met297			Met346			Tyr295			Asn328	Asn328

Reported data are from:
[a] Huang et al. (1994).
[b] Huang et al. (1995); Labrou et al. (2001).
[c] Renzetti et al. (1999).
[d] Meini et al. (2005).
[e] Meini et al. (2004).
[f] Mouillac et al. (1995).
[g] Tahtaoui et al. (2003).
[h] Derick et al. (2004).
[i] Ala334 is the crucial residue for selectivity SR49059 for hV$_{1a}$R over hV$_{1b}$R (Derick et al., 2004).

and C family of GPCRs (Ballesteros et al., 2001; Malherbe et al., 2003, 2006; Petrel et al., 2004). In conclusion, we have demonstrated for the first time the important molecular determinants of NKB, Me-talnetant, and osanetant binding pockets.

References

Albert JS (2004) Neurokinin antagonists and their potential role in treating depression and other stress disorders. *Expert Opin Ther Pat* **14:**1421–1433.

Almeida TA, Rojo J, Nieto PM, Hernandez M, Martin JD, and Candenas ML (2004) Tachykinins and tachykinin receptors: structure and activity relationships. *Curr Med Chem* **11:**2045–2081.

Ballesteros JA and Weinstein H (1995) Integrated methods for construction three-dimensional models and computational probing of structure-function relations in G protein-coupled receptors, in *Methods in Neurosciences*, vol 25, pp 366–428, Academic Press, San Diego, CA.

Ballesteros JA, Shi L, and Javitch JA (2001) Structural mimicry in G protein-coupled receptors: implications of the high-resolution structure of rhodopsin for structure-function analysis of rhodopsin-like receptors. *Mol Pharmacol* **60:**1–19.

Beaujouan JC, Saffroy M, Torrens Y, and Glowinski J (1997) Potency and selectivity of the tachykinin NK3 receptor antagonist SR 142801. *Eur J Pharmacol* **319:**307–316.

Beaujouan JC, Torrens Y, Saffroy M, Kemel ML, and Glowinski J (2004) A 25 year adventure in the field of tachykinins. *Peptides* **25:**339–357.

Cheng Y and Prusoff WH (1973) Relationship between the inhibition constant (K1) and the concentration of inhibitor which causes 50 per cent inhibition (I50) of an enzymatic reaction. *Biochem Pharmacol* **22:**3099–3108.

Dawson LA, Cato KJ, Scott C, Watson JM, Wood MD, Foxton R, de la Flor R, Jones GA, Kew JN, Cluderay JE, et al. (2007) In vitro and in vivo characterization of the non-peptide NK(3) receptor antagonist SB-223412 (talnetant): potential therapeutic utility in the treatment of schizophrenia. *Neuropsychopharmacology*, in press.

Derick S, Pena A, Durroux T, Wagnon J, Serradeil-Le Gal C, Hibert M, Rognan D, and Guillon G (2004) Key amino acids located within the transmembrane domains 5 and 7 account for the pharmacological specificity of the human V1b vasopressin receptor. *Mol Endocrinol* **18:**2777–2789.

Emonds-Alt X, Bichon D, Ducoux JP, Heaulme M, Miloux B, Poncelet M, Proietto V, Van Broeck D, Vilain P, Neliat G, et al. (1995) SR 142801, the first potent non-peptide antagonist of the tachykinin NK3 receptor. *Life Sci* **56:**PL27–PL32.

Giardina GA, Raveglia LF, Grugni M, Sarau HM, Farina C, Medhurst AD, Graziani D, Schmidt DB, Rigolio R, Luttmann M, et al. (1999) Discovery of a novel class of selective non-peptide antagonists for the human neurokinin-3 receptor. 2. Identification of (S)-N-(1-phenylpropyl)-3-hydroxy-2-phenylquinoline-4-carboxamide (SB 223412). *J Med Chem* **42:**1053–1065.

Harrison T, Korsgaard MP, Swain CJ, Cascieri MA, Sadowski S, and Seabrook GR (1998) High affinity, selective neurokinin 2 and neurokinin 3 receptor antagonists from a common structural template. *Bioorg Med Chem Lett* **8:**1343–1348.

Henikoff S and Henikoff JG (1992) Amino acid substitution matrices from protein blocks. *Proc Natl Acad Sci U S A* **89:**10915–10919.

Hoffmann T, Koblet A, Peters J.-U, Schnider P, Sleight A, and Stadler H (2005), inventors; F. Hoffmann-La Roche, Hoffmann T, Koblet A, Peters J.-U, Schnider P, Sleight A, and Stadler H, assignees. Preparation of 2-phenyl-*N*-(pyridin-3-yl)-*N*-methylisobutyramide derivatives as dual NK1/NK3 antagonists for treating schizophrenia. World patent WO2005002577. 2005 Jan 13.

Huang RR, Vicario PP, Strader CD, and Fong TM (1995) Identification of residues involved in ligand binding to the neurokinin-2 receptor. *Biochemistry* **34:**10048–10055.

Huang RR, Yu H, Strader CD, and Fong TM (1994) Interaction of substance P with the second and seventh transmembrane domains of the neurokinin-1 receptor. *Biochemistry* **33:**3007–3013.

Labrou NE, Bhogal N, Hurrell CR, and Findlay JB (2001) Interaction of Met297 in the seventh transmembrane segment of the tachykinin NK2 receptor with neurokinin A. *J Biol Chem* **276:**37944–37949.

Langlois X, Wintmolders C, te Riele P, Leysen JE, and Jurzak M (2001) Detailed distribution of neurokinin 3 receptors in the rat, guinea pig and gerbil brain: a comparative autoradiographic study. *Neuropharmacology* **40:**242–253.

Malherbe P, Kratochwil N, Knoflach F, Zenner MT, Kew JN, Kratzeisen C, Maerki HP, Adam G, and Mutel V (2003) Mutational analysis and molecular modeling of the allosteric binding site of a novel, selective, noncompetitive antagonist of the metabotropic glutamate 1 receptor. *J Biol Chem* **278:**8340–8347.

Malherbe P, Kratochwil N, Muhlemann A, Zenner MT, Fischer C, Stahl M, Gerber PR, Jaeschke G, and Porter RH (2006) Comparison of the binding pockets of two chemically unrelated allosteric antagonists of the mGlu5 receptor and identification of crucial residues involved in the inverse agonism of MPEP. *J Neurochem* **98:**601–615.

Meini S, Catalani C, Bellucci F, Cucchi P, Giuliani S, Zappitelli S, Rotondaro L, Pasqui F, Guidi A, Altamura M, et al. (2005) Pharmacology of an original and selective nonpeptide antagonist ligand for the human tachykinin NK2 receptor. *Eur J Pharmacol* **516:**104–111.

Meini S, Cucchi P, Bellucci F, Catalani C, Faiella A, Rotondaro L, Quartara L,

Giolitti A, and Maggi CA (2004) Site-directed mutagenesis at the human B2 receptor and molecular modelling to define the pharmacophore of non-peptide bradykinin receptor antagonists. *Biochem Pharmacol* **67:**601–609.

Meltzer HY, Arvanitis L, Bauer D, and Rein W (2004) Placebo-controlled evaluation of four novel compounds for the treatment of schizophrenia and schizoaffective disorder. *Am J Psychiatry* **161:**975–984.

Meltzer H and Prus A (2006) NK3 receptor antagonists for the treatment of schizophrenia. *Drug Discov Today Ther Strat* **3:**555–560.

Mouillac B, Chini B, Balestre MN, Elands J, Trumpp-Kallmeyer S, Hoflack J, Hibert M, Jard S, and Barberis C (1995) The binding site of neuropeptide vasopressin V1a receptor. Evidence for a major localization within transmembrane regions. *J Biol Chem* **270:**25771–25777.

Nguyen-Le XK, Nguyen QT, Gobeil F, Pheng LH, Emonds-Alt X, Breliere JC, and Regoli D (1996) Pharmacological characterization of SR 142801: a new non-peptide antagonist of the neurokinin NK-3 receptor. *Pharmacology* **52:**283–291.

Oury-Donat F, Carayon P, Thurneyssen O, Pailhon V, Emonds-Alt X, Soubrie P, and Le Fur G (1995) Functional characterization of the nonpeptide neurokinin3 (NK3) receptor antagonist, SR142801 on the human NK3 receptor expressed in Chinese hamster ovary cells. *J Pharmacol Exp Ther* **274:**148–154.

Palczewski K, Kumasaka T, Hori T, Behnke CA, Motoshima H, Fox BA, Le Trong I, Teller DC, Okada T, Stenkamp RE, et al. (2000) Crystal structure of rhodopsin: a G protein-coupled receptor. *Science* **289:**739–745.

Patacchini R, Bartho L, Holzer P, and Maggi CA (1995) Activity of SR 142801 at peripheral tachykinin receptors. *Eur J Pharmacol* **278:**17–25.

Petrel C, Kessler A, Dauban P, Dodd RH, Rognan D, Ruat M, and Maslah F (2004) Positive and negative allosteric modulators of the Ca^{2+}-sensing receptor interact within overlapping but not identical binding sites in the transmembrane domain modeling and mutagenesis of the binding site of Calhex 231, a novel negative allosteric modulator of the extracellular Ca^{2+}-sensing receptor. *J Biol Chem* **279:**18990–18997.

Renzetti AR, Catalioto RM, Criscuoli M, Cucchi P, Ferrer C, Giolitti A, Guelfi M, Rotondaro L, Warner FJ, and Maggi CA (1999) Relevance of aromatic residues in transmembrane segments V to VII for binding of peptide and nonpeptide antagonists to the human tachykinin NK(2) receptor. *J Pharmacol Exp Ther* **290:**487–495.

Sarau HM, Griswold DE, Bush B, Potts W, Sandhu P, Lundberg D, Foley JJ, Schmidt DB, Webb EF, Martin LD, et al. (2000) Nonpeptide tachykinin receptor antagonists. II. Pharmacological and pharmacokinetic profile of SB-222200, a central nervous system penetrant, potent and selective NK-3 receptor antagonist. *J Pharmacol Exp Ther* **295:**373–381.

Sarau HM, Griswold DE, Potts W, Foley JJ, Schmidt DB, Webb EF, Martin LD, Brawner ME, Elshourbagy NA, Medhurst AD, et al. (1997) Nonpeptide tachykinin receptor antagonists: I. Pharmacological and pharmacokinetic characterization of SB 223412, a novel, potent and selective neurokinin-3 receptor antagonist. *J Pharmacol Exp Ther* **281:**1303–1311.

Severini C, Improta G, Falconieri-Erspamer G, Salvadori S, and Erspamer V (2002) The tachykinin peptide family. *Pharmacol Rev* **54:**285–322.

Sheikh SP, Zvyaga TA, Lichtarge O, Sakmar TP, and Bourne HR (1996) Rhodopsin activation blocked by metal-ion-binding sites linking transmembrane helices C and F. *Nature* **383:**347–350.

Shughrue PJ, Lane MV, and Merchenthaler I (1996) In situ hybridization analysis of the distribution of neurokinin-3 mRNA in the rat central nervous system. *J Comp Neurol* **372:**395–414.

Spooren W, Riemer C, and Meltzer H (2005) Opinion: NK3 receptor antagonists: the next generation of antipsychotics? *Nat Rev Drug Discov* **4:**967–975.

Stoessl AJ (1994) Localization of striatal and nigral tachykinin receptors in the rat. *Brain Res* **646:**13–18.

Tahtaoui C, Balestre MN, Klotz P, Rognan D, Barberis C, Mouillac B, and Hibert M (2003) Identification of the binding sites of the SR49059 nonpeptide antagonist into the V1a vasopressin receptor using sulfhydryl-reactive ligands and cysteine mutants as chemical sensors. *J Biol Chem* **278:**40010–40019.

Tian G, Wilkins D, and Scott CW (2007) Neurokinin-3 receptor-specific antagonists talnetant and osanetant show distinct mode of action in cellular Ca^{2+} mobilization but display similar binding kinetics and identical mechanism of binding in ligand cross-competition. *Mol Pharmacol* **71:**902–911.

Wu LH, Vartanian MA, Oxender DL, and Chung FZ (1994) Identification of methionine134 and alanine146 in the second transmembrane segment of the human tachykinin NK3 receptor as reduces involved in species-selective binding to SR 48968. *Biochem Biophys Res Commun* **198:**961–966.

Address correspondence to: Dr. Pari Malherbe, F. Hoffmann-La Roche Ltd., Bldg. 69/333, CH-4070 Basel, Switzerland. E-mail: parichehr.malherbe@roche.com